INTERNATIONAL ATOMIC ENERGY AGENCY
UNITED NATIONS EDUCATIONAL, SCIENTIFIC AND CULTURAL ORGANIZATION
INTERNATIONAL CENTRE FOR THEORETICAL PHYSICS
I.C.T.P., P.O. BOX 586, 34100 TRIESTE, ITALY, CABLE: CENTRATOM TRIESTE

SMR.703 - 26

WORKING PARTY ON
MECHANICAL PROPERTIES OF INTERFACES

23 AUGUST - 3 SEPTEMBER 1993

"Dislocation-grainboundary Interactions in Ordered Compounds"

"Computer Models and In-situ TEM Observations" Part II - (a) and (b)

J. DE HOSSON
University of Groningen
Department of Applied Physics
Nijenborgh 18
Groningen AG 9747
NETHERLANDS

PART-II-a

PHILOSOPHICAL MAGAZINE A, 1991, VOL. 64, NO. 4, 951-969

Interaction between lattice dislocations and grain boundaries in f.c.c. and ordered compounds: a computer simulation

By B. J. PESTMAN†, J. TH. M. DE HOSSON†, V. VITEK‡
and F. W. SCHAPINK§

† Department of Applied Physics, Materials Science Centre, University of Groningen, Nijenborgh 18, 9747 AG Groningen, The Netherlands
‡ Department of Materials Science and Engineering, University of Pennsylvania, Philadelphia, PA 19104, USA
§ Laboratory of Metallurgy, Delft University of Technology, Rotterdamseweg 137, 2628 AL Delft, The Netherlands

[*Received 3 October 1990 and accepted 12 December 1990*]

ABSTRACT

The interaction of 1/2⟨110⟩ screw- and 60° dislocations with symmetric [110] tilt boundaries was investigated by atomistic simulations using many-body potentials representing a pure f.c.c. metal and ordered intermetallic compounds. The calculations were performed with and without an applied shear stress. The observations were: absorption into the grain boundary, attraction of a lattice Shockley partial dislocation towards the grain boundary and transmission through the grain boundary under the influence of a shear stress. It was found that the structural unit model may help to predict the interaction mechanism for long period boundaries and that the interaction in ordered compounds shows similarities to the interaction in f.c.c. metals. Some comparisons with experimental observations have been made.

§ 1. INTRODUCTION

The structure of grain boundaries determines a number of important properties of polycrystalline materials, among which the mechanical strength is the most affected. Already in the late thirties it was proposed that grain boundaries affect glide of dislocations, i.e. the mechanical properties of polycrystalline materials (Chalmers 1937). A more recent example can be found in a number of ordered compounds, which are very attractive materials for high temperature applications because of their chemical resisitivity and their mechanical strength at high temperatures. These materials are generally ductile as single crystals but show intergranular fracture in their polycrystalline form. This hampers their application, and therefore the physical reason for this intergranular brittleness needs to be scrutinized. A possible answer can be found in the low cohesion of grain boundaries in these materials. However, there is also experimental evidence that the dislocation mobility in the vicinity of grain boundaries may be strongly enhanced when ductilization takes place (Baker, Schulson and Horton 1987). The opposite has been suggested by Chaki (1990). This leads to the conclusion that it is necessary to consider the interaction between dislocations and grain boundaries in detail.

There has been a variety of experimental approaches to the study of dislocation-grain boundary interaction. They include etch-pitting, slip line analysis, and transmission electron microscopy (TEM) (Dingley and Pond 1979). *In situ* deformation in the electron microscope has provided detailed insight in the process of the interaction (Shen, Wagoner and Clark 1988), and additional information on an atomic level has

been provided by high resolution transmission electron microscopy (HRTEM) (Elkajbaji and Thibault-Desseaux 1989). A number of theoretical concepts which help the understanding of the processes at grain boundaries have also been developed, namely the coincidence site lattice (CSL) and displacement-shift-complete lattice (DSC) models (Bollmann 1970, Balluffi, Brokman and King 1982) and the structural unit model (Sutton and Vitek 1983, De Hosson and Vitek 1990).

When a lattice dislocation impinges on a grain boundary, there are various possibilities for the interaction mechanism (Shen, Wagoner and Clark 1988):

(1) The lattice dislocation can dissociate into grain boundary dislocations. A grain boundary dislocation (g.b.d.) can only exist in a grain boundary and a perfect g.b.d. (or DSC dislocation) has a Burgers vector that belongs to the DSC lattice. This mechanism is referred to as absorption.
(2) The lattice dislocation moves into the grain boundary, while another lattice dislocation emerges from the grain boundary into the other grain. A residue with a Burgers vector that is equal to the difference of the two lattice dislocations remains in the boundary. This residue is a DSC dislocation. This mechanism is referred to as transmission.
(3) In addition, there are more complex mechanisms, like absorption and re-emission, at another site in the boundary.

In addition, a grain boundary can be the nucleation site of dislocations.

The selection of the actual interaction mechanism depends on the energetics. In this paper, we focus on the interaction, at the atomic level, between dislocation core and boundary core. The interaction between a number of periodic, symmetric [110] tilt boundaries and dislocations of screw and 60° character with their line direction parallel to [110] was studied by atomistic simulation using two approaches: static simulations (energy minimalization of the combined dislocation and grain boundary system) and kinematical simulations, in which a shear stress is applied in such a way that the dislocation is 'pushed' towards the grain boundary. Two aspects of interest are the application of the structural unit mode to the dislocation-grain boundary interaction and the influence of a high ordering energy on the interaction mechanism.

The simulations were carried out using many-body potentials describing three materials: Cu, Cu_3Au and Ni_3Al. Cu represents a model f.c.c. material, and also can formally be regarded as 'fully disordered' $L1_2$, whereas Cu_3Au represents moderately ordered $L1_2$ (T_c below T_m, the melting temperature) and Ni_3Al represents highly ordered $L1_2$ (T_c above T_m). In this way, the effect of increasing ordering tendency can be studied. The computational procedure is simplified by limiting the choice of systems that are studied to those systems with the dislocation line parallel to the boundary plane, so as to be able to apply periodic boundary conditions along the dislocation line. In this way, little restriction is imposed on small displacements of the dislocation core. Another limitation of the computer simulations is that there there is no possibility of simulating climb of the dislocation. It must be noted that the observations in HRTEM are usually limited to projections of the dislocation line and grain boundary end-on, and a one-to-one comparison with the results of atomistic simulations is possible and will be made.

§2. Method of calculation

For the description of interatomic forces, Finnis–Sinclair potentials representing Cu (Ackland, Tichy, Vitek and Finnis 1987), Cu_3Au (Ackland and Vitek 1989) and

Ni_3Al (Vitek, Ackland and Cserti 1990) were used. For the static simulations, the following procedure was used. First, the grain boundary was relaxed, using a standard gradient method; details are described elsewhere (Sutton and Vitek 1983). In the case of the ordered compounds, different ordering configurations of the grain boundary were considered (see for instance Frost 1987) and the ordering configuration with lowest energy was chosen as a starting point for the dislocation–grain boundary relaxation. Secondly, a computational block for the relaxation of the dislocation near the grain boundary was constructed. The computational block of the grain boundary was extended, according to the periodicity of the CSL, to form a block of 40 **b** × 40 **b** (**b** is the magnitude of the Burgers vector) perpendicular to the tilt axis. Along the tilt axis, periodic boundary conditions were applied. Next, the displacement field of a 1/2⟨110⟩ type dislocation was imposed with its elastic centre near the grain boundary. The anisotropic elastic solution (as if only the upper grain was present) was used for the (fixed) boundary conditions perpendicular to the dislocation line. Of course, the neglect of the presence of the lower grain will introduce a small error in the boundary conditions. The dislocation was introduced in the upper grain at different positions along the grain boundary period, a few lattice parameters away from the grain boundary plane. In the ordered alloys, the displacement field of a 1/2⟨110⟩ type superpartial was imposed with its elastic centre near the boundary plane, connected by a ribbon of anti phase boundary (APB) to another superpartial at elastic equilibrium distance, according to the APB energy. In the case of Cu_3Au the other superpartial was imposed with its elastic centre outside the computational block. Since the elastic equilibrium distance between the two superpartials in Ni_3Al was not as large, the computational block was extended to include both. The dislocation–grain boundary relaxation was carried out in the usual way for dislocation relaxation (Basinski, Duesbery, and Taylor 1970).

For the kinematical simulations, a similar procedure was used, but now the elastic centre of the dislocation was initially positioned at such a distance from the grain boundary that there was no strong effect of the grain boundary on the relaxation of the dislocation core. The initial position of the core was always chosen such that dissociation would occur on the glide plane. After relaxation of the dislocation core, a homogeneous shear strain was imposed on the computational block, corresponding to a shear stress as prescribed by anisotropic elasticity theory (as if only the grain initially containing the dislocation was present). The shear stress was applied in the direction of the Burgers vector, such that the dislocation would move towards the grain boundary plane. The kinematical simulations started with imposing a shear strain corresponding to a small stress. Larger stresses were built up by repeating this process.

§3. Results

Most of the symmetric [110] tilt boundaires studied have (001) as the mean boundary plane. Only the interaction of a 1/2[110] dislocation of pure screw character with these boundaries was simulated. In this set-up, transmission of the dislocation through the grain boundary is relatively easy, as no residue is left behind in the grain boundary plane. In the following, all Miller indices are in the coordinate system of the upper grain, unless indicated otherwise. The $\Sigma = 3$ $(\bar{1}11)$ $(\Theta = 109{\cdot}47°)$ coherent twin boundary and a number of boundaries in the misorientation range 31·59° to 50·48° were relaxed: the $\Sigma = 27$ $(\bar{1}15)$ $(\Theta = 31{\cdot}59°)$; the $\Sigma = 9$ $(\bar{1}14)$ $(\Theta = 38{\cdot}94°)$ (Cu only); the $\Sigma = 57$ $(\bar{2}27)$ $(\Theta = 44{\cdot}0°)$ (Cu only) and the $\Sigma = 11$ $(\bar{1}13)$ $(\Theta = 50{\cdot}48°)$. For Cu, a periodic

pattern of structural units was found: $\Sigma = 3$: C.C; $\Sigma = 27$: A.A; $\Sigma = 9$: AB; $\Sigma = 57$: ABBB; $\Sigma = 11$: B.B, where the . indicates a translation of 1/4 [110] along the tilt axis. For the ordered structure a topologically similar pattern was found, but with two units that differ in the occupation of atom sites by A- and B-atoms. For all materials, the $\Sigma = 27$ and the $\Sigma = 11$ boundaries are favoured boundaries in the misorientation range mentioned, i.e. the boundaries in the intermediate misorientations are composed of the structural units of these boundaries. In the kinematical simulations, the shear stress was applied on the $(1\bar{1}1)$ plane.

The energies of the different ordering states of the boundaries in Cu_3Au and Ni_3Al are given in table 1. The energies of the A_2 and A_3 (and for the $\Sigma = 3$ the A_1, A_2 and A_3) structures should be identical on the basis of symmetry arguments.

Next, the $\Sigma = 9$ $(2\bar{2}1)$ $(\Theta = 38{\cdot}94°)$ boundary with mean plane $(1\bar{1}0)$ was studied (for Cu only). The relaxed boundary has a skew symmetric structure. Simulations were done of the dislocation–grain boundary interaction between this boundary and two types of 60° dislocations, the $1/2[10\bar{1}]$ on the $(1\bar{1}1)$ plane and the $1/2[01\bar{1}]$ on the $(1\bar{1}\bar{1})$ plane. A comparison will be made later with experimental results for Si (Elkajbaji and Thibault-Desseaux 1988).

For a number of boundaries, all low-energy dislocation configurations that have been found for that boundary are represented schematically in figures showing the relaxed boundary structure. It has to be emphasized that the symbols indicating the atom positions are drawn as if there is no dislocation present. Some examples of dislocation structures and the results for the kinematical simulations are depicted using the differential displacement method (Vitek, Perrin and Bowen 1970). This method indicates the relative displacement of each atom with respect to its neighbours in a certain crystallographic direction (usually the direction of the Burgers vector). If the absolute value of the relative displacement exceeds half of the periodicity of the lattice in that direction, an integer number times the period is added or subtracted. In the case of the ordered structure, the periodicity of the f.c.c. structure was used to facilitate the comparison. The position of the APB is indicated by a line. The relative displacements are indicated by arrows drawn between the atoms. In the figures, the regions where the differential displacements have a size between $0{\cdot}30\ a_0$ and $0{\cdot}354\ a_0$ (half the periodicity along the tilt axis, where a_0 is the lattice constant) are indicated by lines; the regions where the differential displacements are between $0{\cdot}15\ a_0$ and $0{\cdot}30\ a_0$ are indicated by lobes (two lines parallel).

Table 1. Grain boundary energies in mJ/m^2 for different ordering states. The cubic sublattices containing the B-atoms are indicated by their relative translation vector (in the coordinate system of the upper grain). The *relaxed* configuration with full symmetry is indicated by S.

Ordering state Translation vector		S [000]	A1 1/2[110]	A2 1/2[101]	A3 1/2[011]
$\Sigma = 3$	Cu_3Au	7	47	47	47
	Ni_3Al	6	208	208	208
$\Sigma = 11$	Cu_3Au	363	344	358	359
	Ni_3Al	506	490	605	606
$\Sigma = 27$	Cu_3Au	697	701	737	737
	Ni_3Al	996	994	1105	1105

3.1. *FCC (Cu)*

In the kinematical simulations, the screw dislocation started to move in the lattice at an applied shear stress of 500 MPa. The screw dislocation was dissociated initially into two Shockley partials in the $(1\bar{1}1)$ plane. Their separation distance was 4 a_0, and they remained separated during the movement.

In the static simulations of the interaction between the screw dislocation and the $\Sigma=3$ boundary one low energy configuration was found: absorption of the screw dislocation and splitting in the boundary plane into two Shockley partial dislocations, the $1/6[12\bar{1}]$ and the $1/6[211]$, which are DSC dislocations of the $\Sigma=3$ boundary, causing a step of $+1$ and -1 interplanar spacing, respectively. See fig. 1.

In the kinematical simulations, the $\Sigma=3$ boundary acted as an obstacle to the motion of the screw dislocation. At a stress level of 500 MPa the screw dislocation started to move towards the boundary plane from its initial position. The leading Shockley partial was halted at the boundary plane and the trailing one remained separated from it by approximately 2 a_0. Upon further increase of the shear stress, this separation distance decreased, and eventually, at 1500 MPa, there was transmission of the screw dislocation through the boundary to the symmetric slip plane in the other grain. See fig. 2. After transmission, the separation of the Shockley's increased again.

For the $\Sigma=27$ boundary, four low energy configurations were found, all showing splitting into two lattice Shockley partial dislocations, on different $\{111\}$ planes, namely the $(\bar{1}11)$ and the $(1\bar{1}1)$ plane. See fig. 3. One of the Shockley partials was always attracted to the boundary and merged into the boundary plane. In most configurations, there was some spreading of the core into the other grain. Some local relaxation effects could be observed. For the kinematical simulations of the $\Sigma=27$ boundary, two

Fig. 1

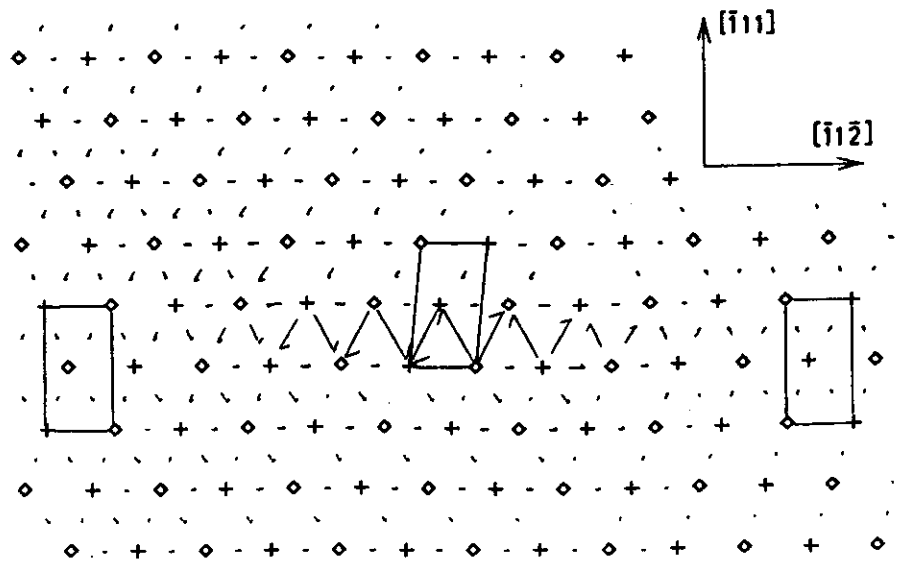

The configuration found for the $\Sigma=3$ boundary in Cu, showing absorption of the screw dislocation in the boundary plane into two g.b.d.s. In this and the following figures, a projection along [110] is shown. The different symbols indicate different heights. Structural units in a boundary are indicated and if a new boundary is formed between the g.b.d.s, structural units in this new boundary are also indicated. The heights indicated by the symbols are heights before the dislocation was imposed.

Fig. 2

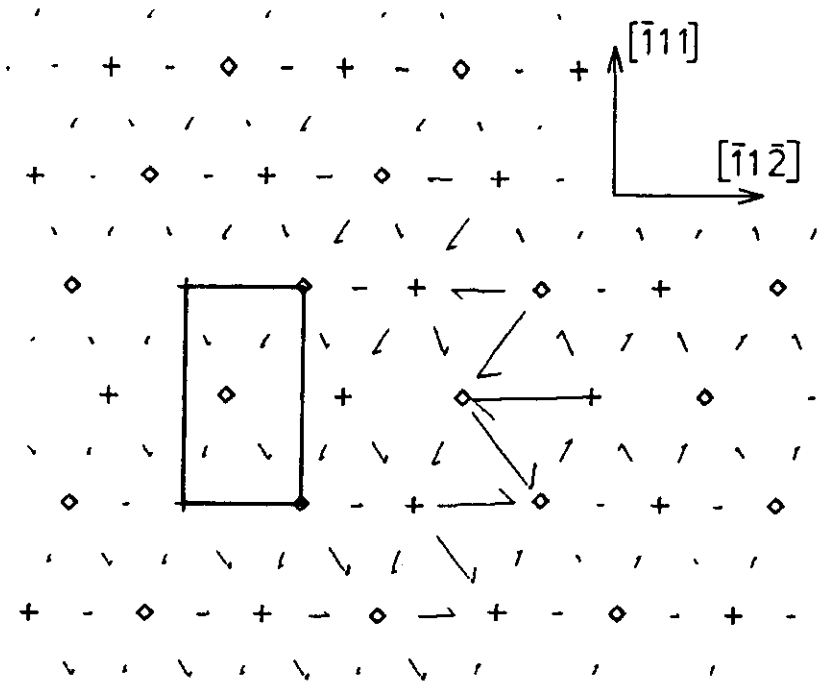

Transmission of the screw dislocation through the $\Sigma=3$ boundary in Cu.

different initial configurations, corresponding to two different $(1\bar{1}1)$ slip planes, ending at different locations in the structural unit, were chosen. In the first case, the screw dislocation reached the boundary in the middle part of the structural unit. Transmission to the $(1\bar{1}\bar{1})_{II}$ plane (the $_{II}$ indicates the coordinate system of the lower grain) occurred at 1300 MPa. Contraction of the two Shockley partials during transmission through the boundary plane was not as pronounced as in the transmission through the $\Sigma=3$ boundary. Strong local relaxation effects could be observed. See fig. 4. In the second case, the $(1\bar{1}1)$ slip plane ended in the left part of the structural unit. The movement of the screw dislocation again started at 500 MPa. Very close to the boundary plane, cross slip to the $(\bar{1}11)$ slip plane occurred and the screw dislocation moved to the right part of the $\Sigma=27$ structural unit. The leading Shockley was absorbed in the grain boundary plane with the trailing Shockley very close behind. When the applied shear stress was increased gradually, the trailing Shockley merged into the boundary plane and the leading one spread its core into the other grain onto the $(1\bar{1}1)_{II}$ plane. No transmission occurred as the simulation continued (the final stress level was 3000 MPa).

The $\Sigma=11$ boundary showed only one low energy configuration: the screw dislocation was absorbed in the boundary and split into two DSC dislocations, the 1/22 $[47\bar{1}]$ and the 1/22 [741]. These DSC dislocations are both glissile in the $(\bar{1}13)$ plane of $\Sigma=11$ boundary. See fig. 5. The two DSCs cause a step of $+1$ and -1 interplanar spacing in the boundary plane respectively. Exactly the same dissociation was found in the kinematical simulations. The screw dislocation started to move towards the boundary at 500 MPa shear stress. At the boundary plane, it dissociated into the two

Fig. 3

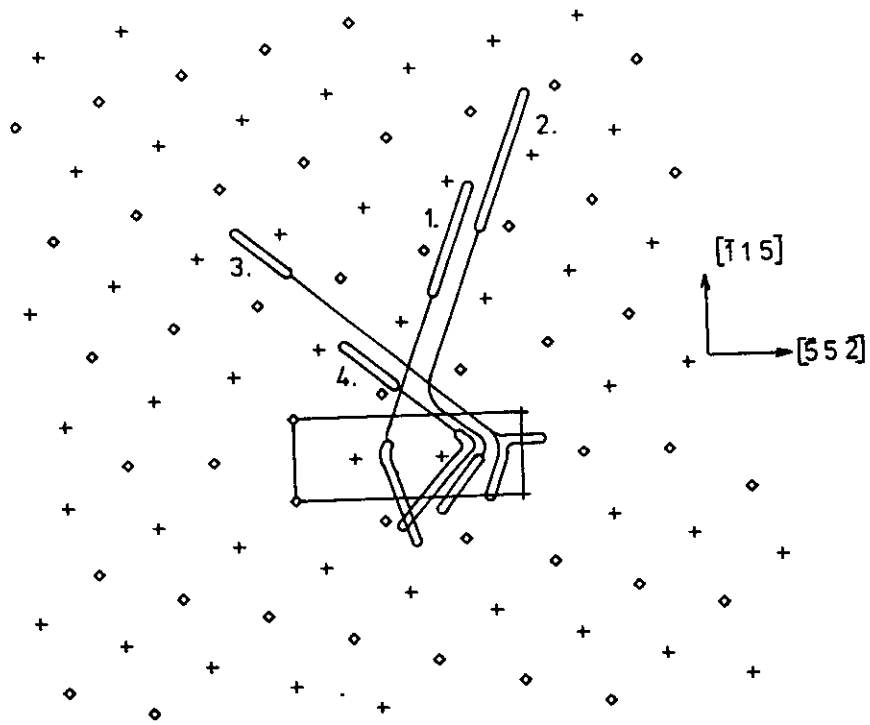

Schematic representation of the configurations found for the $\Sigma=27$ boundary in Cu. All configurations show a Shockley partial dislocation merged in the boundary, connected by a stacking fault to a Shockley in the lattice.

DSC dislocations mentioned above. After the dissociation, the 1/22[741] DSC dislocation moved to the right, to a position close to the border of the computational block.

3.2. *Ordered compounds*

3.2.1. Cu_3Au

In the static simulations for the $\Sigma=3$ boundary two different low energy configurations were found, corresponding to two different types of interaction: one configuration shows absorption into the boundary plane and dissociation into two DSC dislocations of the disordered boundary, the 1/6[12$\bar{1}$] and the 1/6[211], causing a step of one interplanar spacing in the grain boundary plane. The separation between the g.b.d.s was much smaller than the separation in Cu. The part of the new boundary between the g.b.d.s corresponds to a different ordering state of the $\Sigma=3$ boundary. It has to be noted that if the g.b.d.s are moving to different sides of the intersection between APB and boundary plane, two different ordering states of the original boundary are created at the two sides of the APB. These two states differ by the translation vector of the APB. For the boundaries studied in this paper, these have equal energy. The other configuration shows dissociation into two lattice Shockley partial dislocations, one of which was attracted to the boundary. See fig. 6.

The $\Sigma=27$ boundary showed two different types of interaction, with very little energy difference. A number of configurations, which are all examples of the first type of

Fig. 4

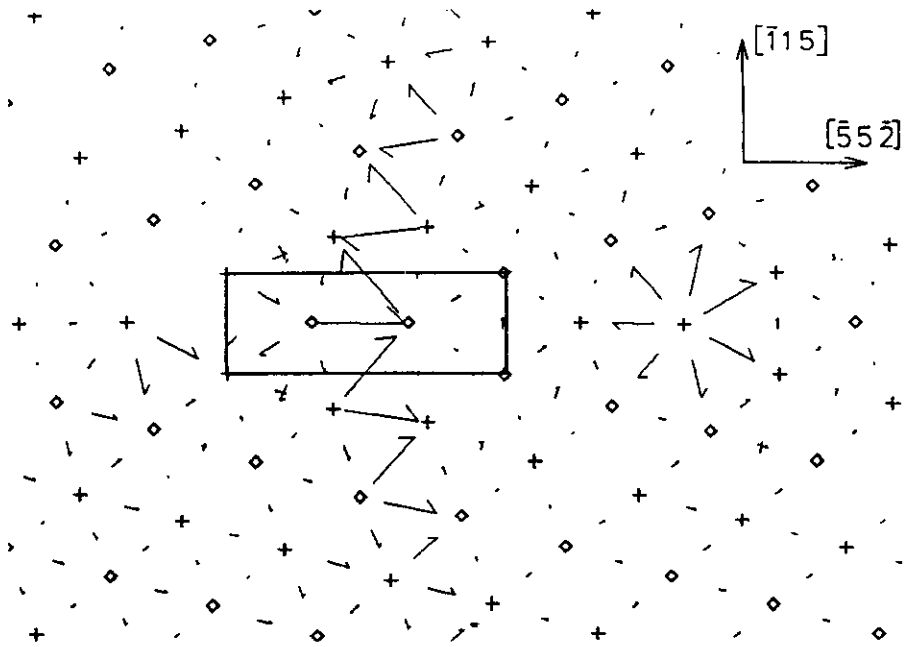

Transmission of the screw dislocation through the middle part of the structural unit of the $\Sigma = 27$ boundary in Cu. Note the strong relaxations in the neighbouring structural units.

Fig. 5

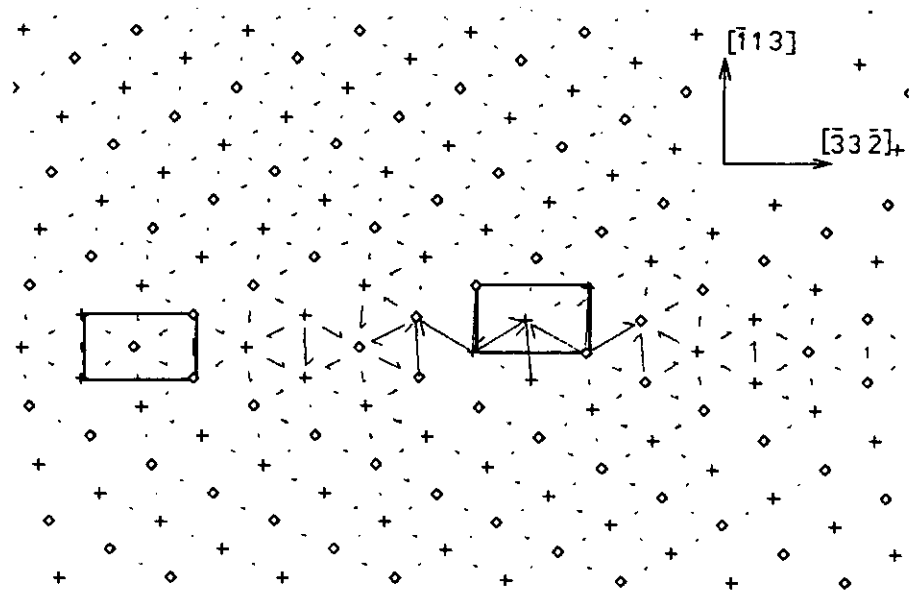

The configuration found for the $\Sigma = 11$ boundary in Cu, showing absorption of the screw dislocation in the boundary plane into two g.b.d.s.

Fig. 6

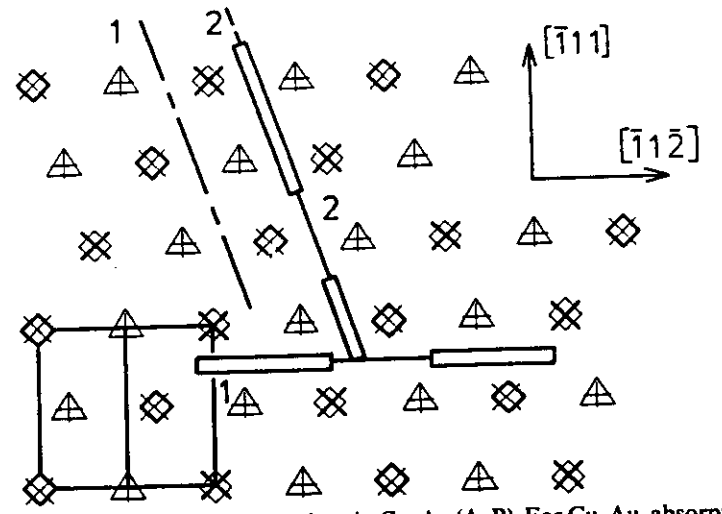

The configurations found for the $\Sigma = 3$ boundary in Cu_3Au (A_3B). For Cu_3Au, absorption in the boundary plane as well as attraction of one Shockley partial dislocation to the boundary plane were found. In this and the following figures, the B-atoms are indicated by thicker lines, with the following order of the symbols: ◇, +, ×, △. The different positions of the APB attached to a configuration are indicated by dashed lines and the number of the configuration.

interaction, showed dissociation into lattice Shockley partial dislocations, one of which was attracted to the boundary. These configurations compare well to the configuration no. 3 of fig. 3 for Cu. In two other configurations (fig. 7), absorption into the boundary plane and dissociation into two DSC dislocations of the disordered boundary, the 1/54[16 11 1] and the 1/54[11 16 $\bar{1}$], was found. The g.b.d.s cause a step in the boundary plane of +4 and −4 interplanar spacings, respectively. The boundary formed between the two cores corresponds to a different ordering state of the original boundary; because of the step in the boundary, some shuffling of atoms has occurred and anti-site defects have been created because of the shuffling.

In the $\Sigma = 11$ boundary, a similar configuration to that in Cu was found again. As the g.b.d.s do not belong to the DSC lattice of the ordered boundary, the part of the boundary between the two g.b.d.s again has an ordering configuration which is different from the original boundary. The separation of the g.b.d.s was smaller than in Cu.

3.2.2. *Ni_3Al*

The relaxation in the perfect lattice of the core of a 1/2[110] superpartial dislocation without an applied shear stress revealed that there were two stable core configurations with very similar energies, depending on the initial position of the core. The first configuration ('glissile') showed spreading of the core on the (1$\bar{1}$1) plane of the APB. The other configuration ('sessile') showed spreading of the core on the ($\bar{1}$11) plane. This result compares well to other simulations in $L1_2$ ordered materials (Yamaguchi, Paidar, Pope, and Vitek 1982, Farkas and Savino 1988). In the kinematical simulations of the interaction with grain boundaries, the initial position of the dislocation was always chosen in such a way, that after the dislocation–grain boundary relaxation the

Fig. 7

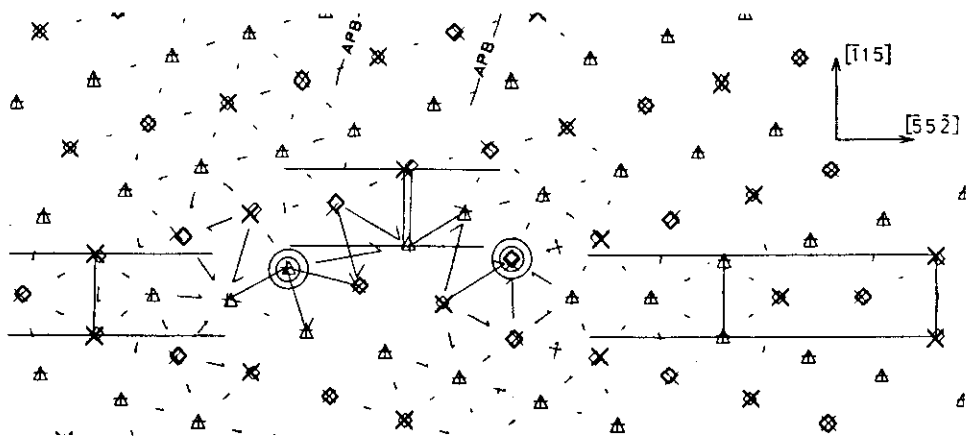

The configuration showing absorption in the boundary plane for the $\Sigma = 27$ boundary in Cu_3Au. The double circles indicate anti-site defects.

glissile core configuration would be attained. In the kinematical simulations in the perfect lattice, the movement of the superpartial screw dislocations started at 700–800 MPa.

In the $\Sigma = 3$ boundary, two different configurations, both similar to the two configurations in Cu_3Au, were found. The separation of the two g.b.d.s in the case of absorption was much smaller than in Cu and this configuration had a slightly higher energy than the configuration showing dissociation into two lattice Shockley partials. The interaction of the 1/2[110] superpartial screw dislocation with the $\Sigma = 3$ boundary in the kinematical simulations showed a similar mechanism to Cu. The leading superpartial was dissociated into two Shockley partials with very small separation. Upon arrival at the boundary plane, the leading Shockley partial was stopped and a slight decrease of the separation of the Shockleys could be observed. When the shear stress reached a level of 2900 MPa, transmission occurred across the boundary into the symmetric slip plane in the other grain.

For the $\Sigma = 27$ boundary only one type of interaction was found: dissociation into lattice Shockley partials, with one partial merged into the boundary. Most of the configurations that were found compare well with the configurations nos. 1, 3 and 4 of fig. 3 for Cu. One new configuration (no. 3 of fig. 8) was found for Ni_3Al; this configuration had a slightly higher energy. See fig. 8.

For the study of the interaction with the $\Sigma = 27$ boundary in the kinematical simulations, two different initial configurations were chosen. In the first configuration, the (1$\bar{1}$1) slip plane of the superpartial ended in the middle of structural unit no. 1. See fig. 9(*a*). When the leading 1/2[110] superpartial reached the boundary, it was halted, with one Shockley merged into the boundary plane and the other in the lattice, very close to the boundary plane. When the stress level increased, the Shockley partial in the lattice gradually spread its core onto the ($\bar{1}$11) plane. At a stress level of 3400 MPa, the Shockley partial (originally 1/6[121]) had dissociated into a 1/6[$\bar{1}$10] stair rod dislocation, located approximately at the original position of the Shockley, and a new Shockley partial, 1/6[211], which had merged into the right part of structural unit no. 2.

Fig. 8

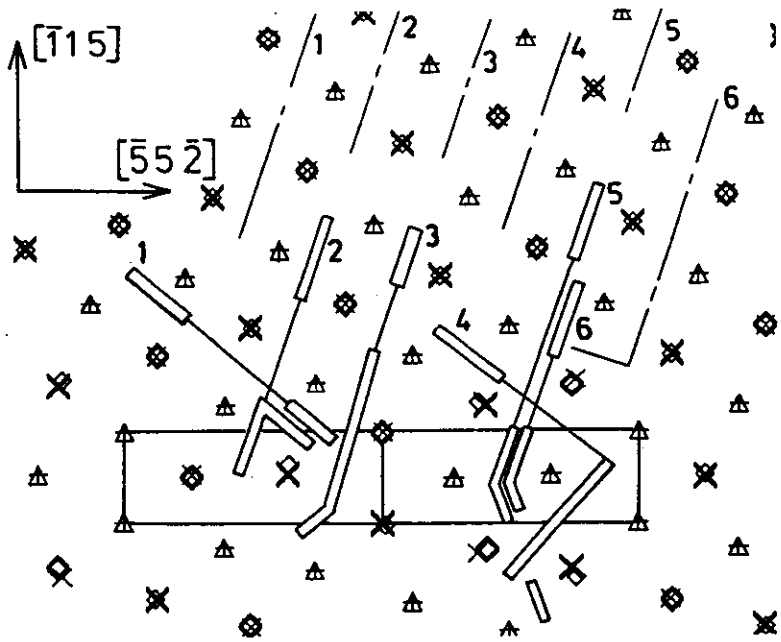

The configurations found for the $\Sigma=27$ boundary in Ni_3Al.

In this way, a new, second region of complex stacking fault (CSF) had formed on the $(\bar{1}11)$ plane, connecting the stair rod dislocation and the newly formed Shockley partial. See fig. 9(*a*). At a stress level of 3900 MPa, the trailing 1/2[110] superpartial approached the configuration and a reaction between the stair rod dislocation and the leading Shockley of this superpartial took place, in which the $1/6[12\bar{1}]$ Shockley partial was created. The $1/6[12\bar{1}]$ Shockley partial cross-slipped away along the $(\bar{1}11)$ plane, thus creating an APB on the $(\bar{1}11)$ plane. Finally, at a stress level of 4200 MPa, a CSF was formed on a $(1\bar{1}\bar{1})_{II}$ plane in the other grain. See fig. 9(*b*). In the second configuration, the slip plane of the superpartial ended in the left part of structural unit no. 2. The superpartial cross slipped onto the $(\bar{1}11)$ plane and merged into the right part of the structural unit, analogous to the second mechanism described for the interaction with the $\Sigma=27$ boundary in Cu. At an applied shear stress of 3100 MPa, the superpartial was transmitted into the other grain onto a $(1\bar{1}\bar{1})_{II}$ plane. See fig. 10.

The $\Sigma=11$ boundary again showed the same configuration as was found in Cu_3Au. The separation between the g.b.d.s was smaller than the separations in Cu and Cu_3Au. In the kinematical simulations, one Shockley partial was initially attracted to the boundary while the other remained in the lattice at $3\,a_0$ from the boundary plane. Thus, a relatively large area of CSF was created. When the stress level was increased further, this configuration remained the same, with only a slight decrease in the separation of the Shockley partials, until a stress level of 1900 MPa was reached. At this level, the superpartial was absorbed in the boundary and split into two g.b.d.s belonging to the DSC lattice of the disordered boundary, analogous to the mechanism in Cu.

Fig. 9

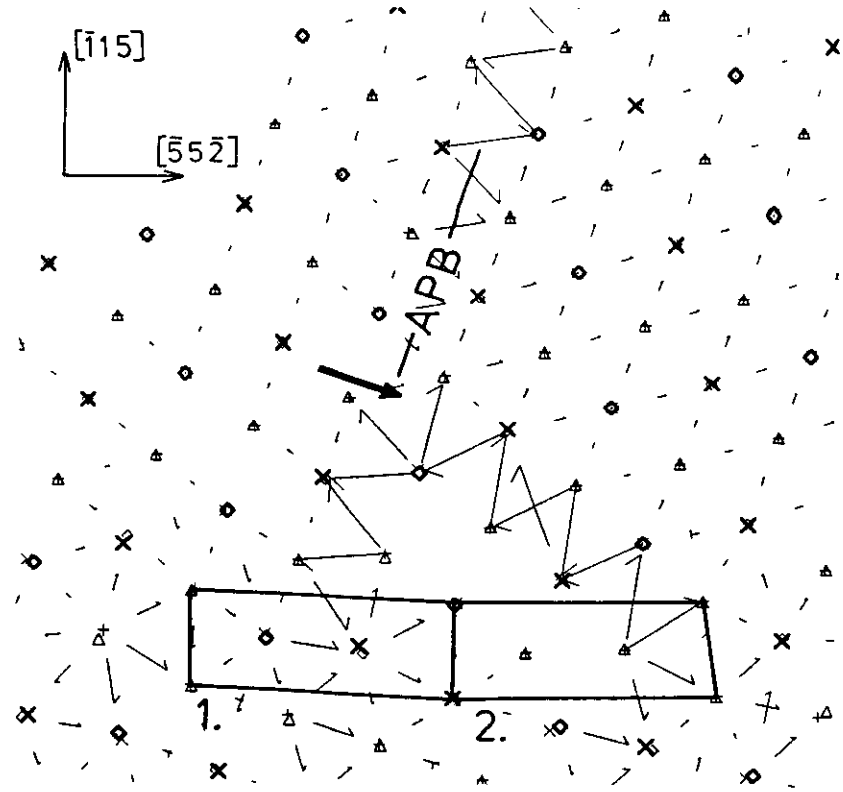

(*a*)

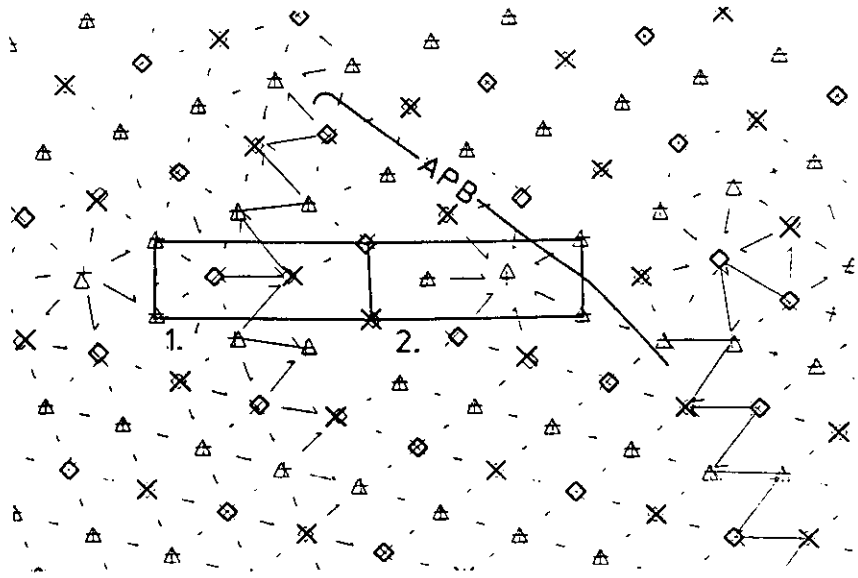

(*b*)

(*a*) First stage of the interaction with the $\Sigma=27$ boundary in Ni_3Al in the kinematical simulations. Both the leading and the trailing superpartial dislocations are visible. The arrow indicates the position of the stair rod dislocation. (*b*) Final configuration. The trailing superpartial has cross-slipped to the right and a CSF has been created in the lower grain.

Fig. 10

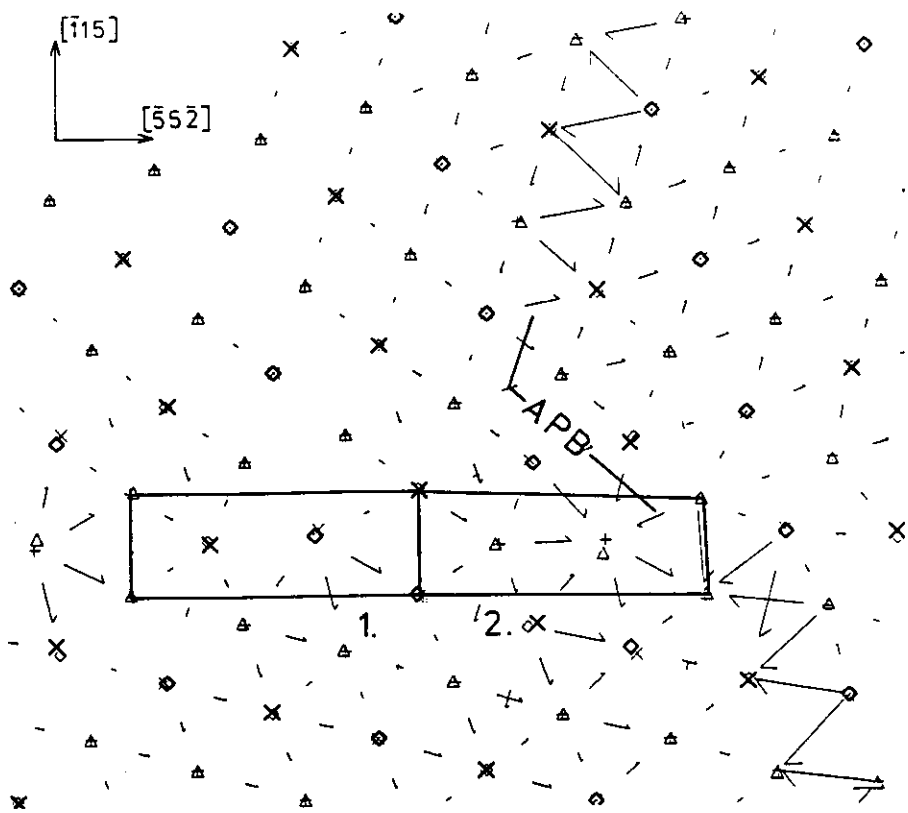

Transmission of the leading superpartial through the $\Sigma = 27$ boundary in Ni_3Al. The trailing superpartial is visible in the upper grain.

3.3. *Structural unit model and comparison with experiment*

In the structural unit model, the structure of grain boundaries in the misorientation range between two low energy boundaries can be described as composed of a sequence of building blocks or 'structural units' of these two 'favoured' boundaries. In our case, the $\Sigma = 27$ and the $\Sigma = 11$ boundary are the favoured boundaries and the $\Sigma = 57$ and $\Sigma = 9$ $(\bar{1}14)$ boundary are composed of units of the $\Sigma = 27$ and $\Sigma = 11$ boundaries. The interaction of a 1/2[110] screw dislocation with the $\Sigma = 57$ and $\Sigma = 9$ boundaries was studied in Cu.

The low energy configurations for the $\Sigma = 57$ boundary are very similar to those found for the two delimiting favoured boundaries. In the parts of the boundary that can be described by $\Sigma = 11$ units, the mechanism of absorption in the boundary was observed again. The splitting was never beyond the two $\Sigma = 27$ units on both sides of the $\Sigma = 11$ region. For the $\Sigma = 27$ units, three of the four configurations that had been found for the $\Sigma = 27$ boundary were found here again. See fig. 11. The $\Sigma = 9$ $(\bar{1}14)$ boundary again showed configurations that were similar to the $\Sigma = 11$ and $\Sigma = 27$ boundaries. Although the boundary consists of a repeating sequence of only one $\Sigma = 11$ and one $\Sigma = 27$ structural unit, the mechanism of absorption into the $\Sigma = 11$ unit was observed here again; the splitting in the boundary plane was limited to the very narrow region of

Fig. 11

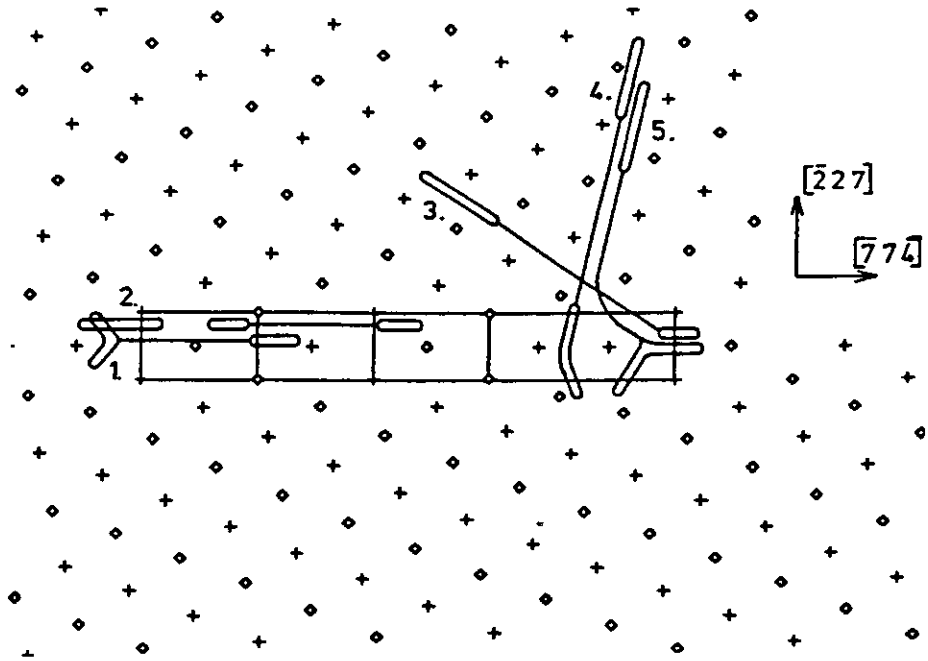

The configurations found for the $\Sigma = 57$ boundary in Cu, showing similarity to the configurations found for the $\Sigma = 27$ and $\Sigma = 11$ delimiting favoured boundaries.

Fig. 12

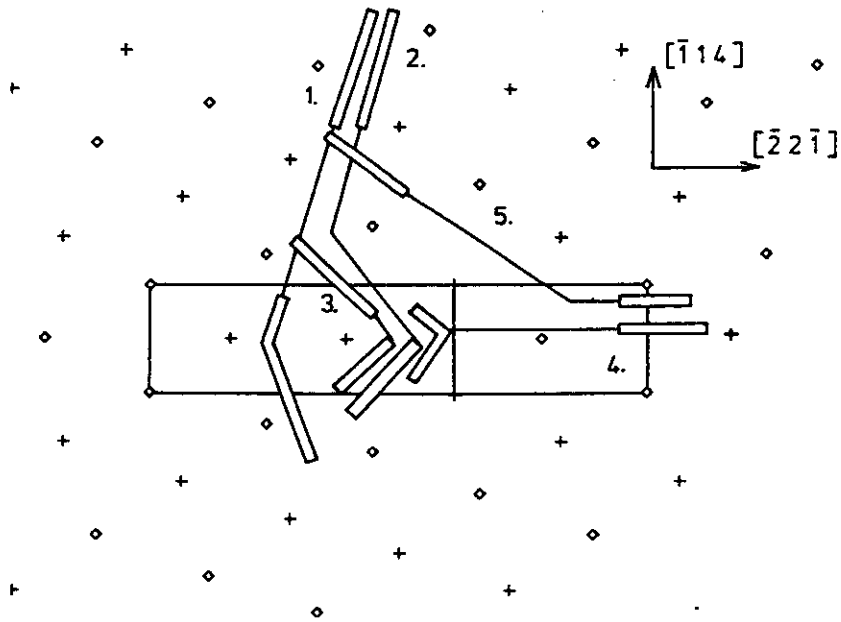

Schematic figure of the configurations found for the $\Sigma = 9$ ($\bar{1}14$) boundary in Cu, showing mostly similarities to the configurations found for the $\Sigma = 27$ and $\Sigma = 11$ delimiting favoured boundaries.

Fig. 13

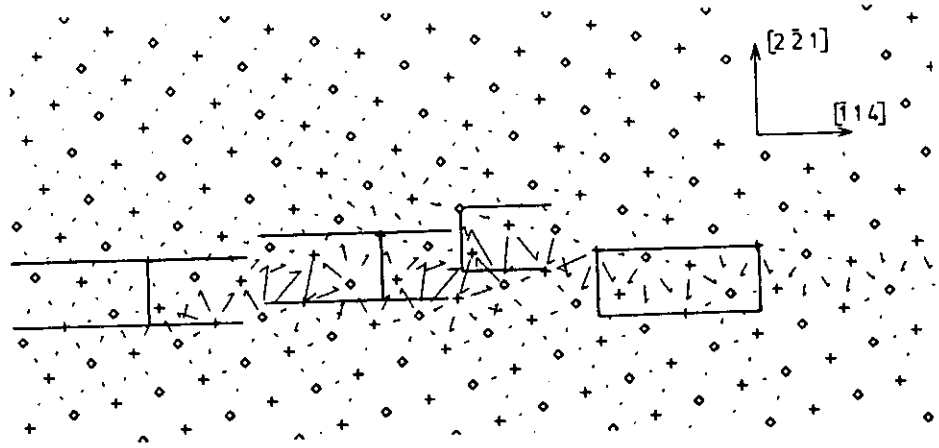

Absorption of the 1/2[10$\bar{1}$] 60° dislocation in the $\Sigma=9$ (2$\bar{2}$1) boundary into two 1/18[1$\bar{1}$4] and one 1/18[72$\bar{1}$] g.b.d.s in Cu. In this figure, the displacements parallel to the 1/18[1$\bar{1}$4] DSC dislocation are indicated.

one $\Sigma=11$ unit. The occurrence of one extra configuration (no. 5 of fig. 12) shows that there was some interference between the $\Sigma=11$ and the $\Sigma=27$ units. See fig. 12.

A number of simulations of the interaction of 60° dislocations with the $\Sigma=9$ (2$\bar{2}$1) boundary were performed to be able to compare with experimental observations. The simulations for the interaction between the $\Sigma=9$ (2$\bar{2}$1) boundary and the 1/2[10$\bar{1}$] 60° dislocation on the (1$\bar{1}$1) plane show absorption of the dislocation and splitting into the 1/18 [22$\bar{8}$] and 1/18[72$\bar{1}$] DSC dislocations, causing an effective step (King and Smith 1980) in the boundary plane of +4 and −3·5 interplanar layers, respectively. The 1/18[22$\bar{8}$] DSC is not an elementary DSC dislocation and it is glissile in the boundary plane, so it could be expected to split into two 1/18 [1$\bar{1}$4] dislocations. If the initial configuration before relaxation was altered in such a way that the position of the boundary plane was displaced by 4 interplanar spacings over a length of 2 boundary periods by shuffling of the atoms in these planes, a different configuration with lower energy was observed, showing splitting into two separate 1/18[1$\bar{1}$4] dislocations and the 1/18[72$\bar{1}$]. See fig. 13. For the interaction with the 1/2[01$\bar{1}$] dislocation on the (1$\bar{1}$1) plane, splitting into lattice Shockley partials was observed and the leading (pure edge) partial was attracted to the boundary plane.

§4. Discussion

In all the examples studied so far, there was an attractive force between the boundary and the (partial) dislocation core. First, we will discuss the results of the static simulations for the $\Sigma=3$, the $\Sigma=27$ and the $\Sigma=11$ boundaries and we will consider the effect of increasing ordering tendency.

For the $\Sigma=3$ and the $\Sigma=11$ boundaries, the absorption in the boundary plane and splitting into DSC dislocations can be understood using the $\mathbf{b}^2$ criterion, the fact that both dislocations are glissile in the boundary plane, the small step height associated with these dislocations and the conservation of step height (King and Smith 1980). In Cu, the new boundary that is formed between the two g.b.d.s is exactly the same as the original boundary, and therefore, from an elastic point of view, the g.b.d.s would be

expected to move apart as far as possible. Recent simulations using Finnis–Sinclair potentials (Pestman, De Hosson, Vitek, Tichelaar and Schapink 1990) show that the friction stress for screw dislocations is high in perfect crystal. An estimate of the elastic repulsion (using bulk elastic constants and isotropic elastic theory) in equilibrium with the friction stress yields a separation distance which is comparable to the actual separation that was found in the simulations described in this paper. As the Burgers vectors of the DSC dislocations in the $\Sigma = 11$ boundary are more parallel than those in the $\Sigma = 3$ boundary, a stronger elastic repulsion between them, and hence a large separation distance between the $\Sigma = 11$ g.b.d.s, would be expected. A possible reason why this is not so, might be found in a higher friction stress for glide in the $(\bar{1}13)$ boundary plane of the $\Sigma = 11$ boundary than for the $(\bar{1}11)$ boundary plane of the $\Sigma = 3$. The results for the $\Sigma = 3$ and $\Sigma = 11$ boundaries are confirmed by experimental observations using TEM of widely dissociated pairs of the same DSC dislocations in austenitic stainless steel for $\Sigma = 3$ (Pumphrey and Bowkett 1971) and for $\Sigma = 11$ by *in situ* observations of DSC dislocations, to which the same Burgers vectors are attributed as in our case, gliding on the $(\bar{1}13)$ boundary plane in Al (Mori and Tangri 1979).

The decrease in separation of the g.b.d.s when we go from 'disordered' Cu via Cu_3Au to strongly ordered Ni_3Al can be explained by the differences in the energy of the new grain boundary segment that is created between the g.b.d.s. The energy difference between the original boundary and the boundary created between the g.b.d.s is zero for disordered material and increases with increasing ordering tendency. See also table 1. In Cu_3Au and in Ni_3Al, a stable configuration showing splitting into two lattice Shockley particals occurred for the $\Sigma = 3$ boundaries in contrast to Cu where this did not occur. This can be explained by the small differences between the energy of the CSF, which is created between the two lattice Shockley partials, and the ordering fault energy of the boundary that is created between the g.b.d.s in the case of absorption. If we assume bulk elastic constants and only take the energy of the fault that is created between the two g.b.d.s into account, the equilibrium separation using isotropic elastic theory of the two g.b.d.s in the $\Sigma = 11$ in Ni_3Al, for example, would be expected to be $5{\cdot}1\ a_0$. The high friction force again could be the reason for the smaller splitting distances that are observed in the simulations.

In the $\Sigma = 27$ case, the attraction without splitting into g.b.d.s in the boundary plane shows that the (partial) dislocation core can lower its energy by merging into the boundary core. Absorption into DSC dislocations, as occurred in Cu_3Au structure, causes a larger step in the grain boundary plane than in the $\Sigma = 11$ or $\Sigma = 3$ boundary and glide of the two DSC dislocations will be associated with shuffling of atoms. Also, in the $L1_2$ structure, depending on the way the shuffling takes place, anti-site defects can be created in the shuffled region (i.e. the region between the positions of the boundary plane before and after migration). This will limit the separation of DSC dislocations. This argument can be applied in general to boundaries in the ordered structure. Even for another grain boundary-dislocation system, if there is dissociation into g.b.d.s that belong to the DSC lattice of the ordered grain boundary and no fault in the new boundary structure between the g.b.d.s is created, the creation of anti-site defects will limit the separation of the g.b.d.s. The reason why the splitting into g.b.d.s only occurred in Cu_3Au, might be found in the differences in the interatomic interactions between the three materials.

Now we turn to the results of the kinematical simulations. The applied shear stresses necessary to start the movement of the screw dislocations in perfect lattice are

0·009 μ for Cu (μ is the shear modulus) and 0·007 μ for Ni_3Al. These values are high in comparison to experimental values of the friction stress, even if we take into account the fact that the simulations are done at 0 K and that the friction stress for a screw dislocation is higher than for an edge. Of course, it should be noted that, because of the periodic boundary conditions along the dislocation line, motion of the screw dislocation through the formation of kinks is prohibited.

The transmission through the $\Sigma = 3$ boundary in both materials can be explained by the small angle between the symmetric slip plane in the other grain and the original slip plane, and consequently a high resolved shear stress on this slip plane. Transmission occurred at three times the friction stress for Cu and four times the friction stress for Ni_3Al, indicating that the $\Sigma = 3$ boundary is a stronger obstacle to dislocation movement in Ni_3Al.

From the study of the interaction with the $\Sigma = 27$ boundary in Cu, it can be concluded that the interaction with a boundary can show large differences, depending on where the dislocation arrives in the boundary. The resistance against shear seems to depend on the local atomic configuration and the differences within a structural unit can be large. When we compare the results for Cu and Ni_3Al, there are large differences between the interaction of the screw dislocation with the middle part of the structural unit in Cu and the interaction of the superpartial with the middle part of structural unit no. 1 in Ni_3Al. In Cu, transmission is observed at a stress level of less than three times the friction stress, while in Ni_3Al at more than five times the friction stress a complicated reaction takes place and transmission occurs at a different location in the grain boundary. When we compare the interaction of the screw dislocation gliding towards the left part of the structural unit in Cu with the interaction of the superpartial gliding towards the left part of structural unit no. 2 in Ni_3Al, we observe the same mechanism of cross slip towards the right part of the structural unit.

Both the $\Sigma = 3$ and the $\Sigma = 27$ boundaries show a tendency to transmission under an applied shear stress. In Ni_3Al, however, the stress level at which transmission occurs is clearly higher, even in terms of the friction stress, and the boundaries prove to be strong obstacles against passage of dislocations. It could be reasoned that a superdislocation arriving at a grain boundary in Cu_3Au and especially in Ni_3Al with its high APB energy first responds to an applied shear stress by decreasing the width of the APB separating the two superpartials. As a matter of course this phenomenon does not occur in f.c.c. Cu and, consequently, the boundaries are more transparent for moving dislocations. In Ni_3Al in particular, the close approach of the trailing superpartial to the leading one causes a stress concentration at the boundary plane. It might be envisaged that in reality in Ni_3Al, other processes like intergranular fracture will occur in response to the applied stress at lower stress levels than those necessary for transmission.

The absorption in the $\Sigma = 11$ boundary compares well to the static simulations, for in those the tendency of absorption and splitting into DSC dislocations was observed in both materials. This tendency is presumably so strong that transmission onto the $(1\bar{1}\bar{1})_{II}$ plane does not occur, in spite of the small deviation angle with respect to the original slip plane.

The results for the $\Sigma = 57$ and the $\Sigma = 9$ $(\bar{1}14)$ boundaries show that the structural unit model may help us to predict the interaction between the screw dislocation and a long period boundary, if we know the interaction between the dislocation and the delimiting favoured boundaries. The results of a previous pair potential study of the $\Sigma = 57$ boundary in $L1_2$ ordered structure (Pestman, De Hosson, Vitek and Schapink 1990) suppport this conclusion for ordered alloys. However, there are two consider-

ations that have to be kept in mind: first, in the case of absorption in the boundary and splitting into DSC dislocations, the distance of splitting is limited to one type of structural unit; second, the minority units can be thought to contain a dislocation core and there can be elastic interaction with the lattice dislocation. In our case, the core of the $1/22[\bar{2}26]$ DSC that can be considered to be located in the $\Sigma=27$ unit in the $\Sigma=57$ boundary has elastic interaction with the edge components of the Shockley partials in the $(1\bar{1}1)$ plane of the screw dislocation. The leading partial is attracted whereas the trailing one is repelled. This might be an explanation for the slightly larger stacking fault of configurations no. 4 and 5 of fig. 11 for $\Sigma=57$ with respect to the configurations no. 1 and 2 of fig. 3 for $\Sigma=27$.

The simulations for the $\Sigma=9(2\bar{2}1)$ boundary in Cu can be compared with HRTEM observations of Elkajbaji and Thibault-Desseaux (1988) of the same system in Si. Since Si can be regarded as an f.c.c. lattice with a basis consisting of two atoms, the geometry of the system is the same. The splitting of the $1/2[10\bar{1}]$ dislocation into the $1/18[72\bar{1}]$ (which is the $1/6[21\bar{1}]_{II}$ in the notation as used by Elkajbaji and Thibault) and two $1/18[1\bar{1}4]$ g.b.d.s compares very well with fig. 9 of their paper. In our simulations the splitting distances are much lower, as the friction stress in the simulations is relatively high. The attraction to the grain boundary plane of the leading 90° Shockley partial of the $1/2[011]$ lattice dislocation compares well with fig. 8 (*a*) of their paper. Splitting of the leading Shockley partial into two g.b.d.s, as was observed experimentally, would not be expected to occur in the simulations: there is no driving force for this dissociation, because the Burgers vectors of the two g.b.d.s are perpendicular and in the simulations there are no external stresses.

The simulations have been done for configurations at 0 K. It could be reasoned that the mechanisms of the interactions, which are mostly derived from calculations of energy differences, will probably remain the same at higher temperatures, whereas the motion of the g.b.d.s, especially if associated with shuffling atoms or with climb, will be easier. Further, the concept of structural multiplicity has been found to be very common within the structural unit model, with alternative structures frequently possessing very similar energies. The existence of these alternative structures suggests that at high temperatures transformations of the boundary structures could occur. These transformations may either be of the order–disorder type involving transition from a periodic to a non-periodic multiple structure, or the transitions from one alternative structure to another (Vitek, Minonishi, Wang 1985, Vitek and De Hosson 1986).

§5. Conclusions

(1) A number of experimental observations of dislocation–grain boundary interaction can be reproduced in computer simulation.

(2) The structural unit model may be used to predict the interaction of a lattice dislocation with boundaries in a certain misorientation range if the interaction of the lattice dislocation with the favoured boundaries delimiting the misorientation range is known.

(3) The mechanism of the interaction between lattice dislocations and grain boundaries is similar for boundaries in ordered and disordered (or f.c.c.) materials. In the case of absorption into g.b.d.s in ordered material, an ordering fault is left behind in the boundary plane and anti-site defects may be created during movement of the g.b.d. Because of these phenomena, movement of g.b.d.s in ordered material is hindered and, in the case of extended slip, stress

concentrations will develop at the boundary upon arrival of more lattice dislocations. In the case of transmission, the simulations show that transmission through an ordered boundary occurs at high stress levels and the superpartials constituting the arriving dislocation will decrease their separation in response to the applied stress. In this way, stress concentrations near the boundary will be generated. These considerations suggest that the interaction between lattice dislocations and grain boundaries may be of importance for the explanation of the intergranular fracture occurring in a number of ordered compounds, particularly those with a high ordering energy.

ACKNOWLEDGMENTS

This work is part of the research program of the Foundation for Fundamental Research on Matter (F.O.M.-Utrecht) and has been made possible by financial support from the Netherlands Organization for Research (N.W.O.-The Hague). A support of the National Science Foundation, MRL Program under Grant no. DMR88-19885 (VV) is acknowledged.

REFERENCES

ACKLAND, G. J., TICHY, G., VITEK, V., and FINNIS, M. W., 1987, *Phil. Mag.* A, **56**, 735.
ACKLAND, G. J., and VITEK, V., 1989, *High Temperature Ordered Intermetallic Alloys*, edited by C. C. Koch, C. T. Liu and A. I. Taub (Mater. Res. Soc. Symp. Proc. 133), p. 105.
BAKER, I., SCHULSON, E. M. and HORTON, J. A., 1987, *Acta Metall.*, **35**, 1533.
BALLUFFI, R. W., BROKMAN, A., and KING, A. H., 1982, *Acta Metall.*, **30**, 1453.
BASINSKI, Z. S., DUESBERY, M. S., and TAYLOR, R., 1970, *Phil. Mag.*, **21**, 1201.
BOLLMANN, W., 1970, *Crystal Defects and Crystalline Interfaces* (Berlin: Springer).
CHAKI, T. K., 1990, *Phil. Mag. Lett.*, **61**, 5.
CHALMERS, B., 1937, *Proc. R. Soc. London.* A, **162**, 120.
DE HOSSON, J. TH. M., and VITEK, V., 1990, *Phil. Mag.* A, **61**, 305.
DINGLEY, D. J., and POND, R. C., 1977, *Acta Metall.*, **27**, 667.
ELKAJBAJI, M., and THIBAULT-DESSEAUX, J., 1988, *Phil. Mag.* A, **58**, 325.
FARKAS, D., and SAVINO, E. J., 1988, *Scripta Metall.*, **22**, 557.
FROST, H., 1987, *Acta Metall.*, **35**, 519.
KING, A. H., and SMITH, D. A., 1980, *Acta Crystallogr.* A, **36**, 335.
MORI, T., and TANGRI, K., 1979, *Metall. Trans.* A, **10**, 733.
PESTMAN, B. J., DE HOSSON, J. TH. M., VITEK, V., and SCHAPINK, F. W., 1990, *J. de Phys. Paris*, **51**, C1-311.
PESTMAN, B. J., DE HOSSON, J. TH. M., VITEK, V., TICHELAAR, F. D., and SCHAPINK, F. W., 1990, *Alloy Phase Stability and Design*, edited by G. M. Stocks, D. P. Pope and A. F. Giamei (Mater. Res. Soc. Symp. Proc., MRS 186).
PUMPHREY, P. H., and BOWKETT, K. M., 1971, *Phil. Mag.* A, **24**, 225.
SHEN, Z., WAGONER, R. H., and CLARK, W. A. T., 1988, *Acta Metall.*, **36**, 3231.
SUTTON, A. P., and VITEK, V., 1983, *Philos. Trans. R. Soc. London* A, **309**, 37.
VITEK, V., ACKLAND, G. J., and CSERTI, J., 1990, *Alloy Phase Stability and Design*, edited by G. M. Stocks, D. P. Pope and A. F. Giamei (Mater. Res. Soc. Symp. Proc., MRS 186).
VITEK, V., and DE HOSSON, J. TH. M., 1986, *Computer-based Microscopic Description of the Structure and Properties of Materials*, edited by J. Broughton, W. Krakow and S. T. Pantelides, MRS 63, 137.
VITEK, V., MINONISHI, Y., WANG, G.-J., 1985, *J. Physique*, **46**, C4-171.
VITEK, V., PERRIN, R. C., and BOWEN, D. K., 1970, *Phil Mag.*, **21**, 1049.
YAMAGUCHI, M., PAIDAR, V., POPE, D. P., and VITEK, V., 1982, *Phil. Mag.* A, **45**, 867.

PART-II
-6

Reprinted from

ACTA METALLURGICA ET MATERIALIA

Vol. 40, No. 10, pp. 2511–2521

INTERACTIONS BETWEEN LATTICE DISLOCATIONS AND GRAIN BOUNDARIES IN Ni_3Al INVESTIGATED BY MEANS OF *IN SITU* TEM AND COMPUTER MODELLING EXPERIMENTS

B. J. PESTMAN and J. Th. M. DE HOSSON

Department of Applied Physics, Materials Science Center, University of Groningen, Nijenborgh 18, 9747 AG Groningen, The Netherlands

PERGAMON PRESS LTD

OXFORD · NEW YORK · SEOUL · TOKYO

1992

ordered compounds are ever to be further developed, it is useful to scrutinize the reasons for their brittle behaviour. A possible reason could be found in low cohesion of the grain boundaries.

However, there exists experimental evidence that in Ni$_3$Al the dislocation mobility in the vicinity of grain boundaries may be strongly enhanced when ductilization takes place [2] and that plastic flow precedes inter-granular fracture [3]. Considering these experiments, it might be reasoned that the passage of gliding dislocations arriving from the lattice might be hindered by grain boundaries. The results of computer modelling studies [4–5] indicate that grain boundaries in $L1_2$ ordered compounds hinder dislocation motion. This effect increases with higher ordering tendency.

Various approaches exist to the experimental study of the interaction between lattice dislocations and grain boundaries, such as slip line analysis [6] and etch-pitting [7]. However, these techniques are not capable of giving information about the nature of the dislocation and the grain boundary, such as the line direction and the Burgers vector of a dislocation, the orientation of the grain boundary plane and the misorientation between the two grains. Transmission electron microscopy is a technique that allows observation of defect configurations in thin foils and also provides information of the nature of the defects. In many experiments [8, 9], bulk samples of different materials have been deformed and these samples have been prepared for study in the TEM. Although a full analysis of the dislocation–grain boundary configuration is possible, the development of the interaction has to be deduced from the configuration that is left behind after the interaction has taken place.

In situ deformation in a TEM is one of the very few techniques by which the development of the interaction between lattice dislocations and grain boundaries can be studied and which at the same time allows to analyze the configuration. By this technique, samples which have not yet been deformed, are strained inside a TEM in a special straining holder. In practice there are a number of complexities. It is always possible that there is a substantial influence of the fact that the interaction is studied in a very thin foil, while we are interested in bulk properties: the electron transparent region may have a complicated geometry because of the thinning and therefore the stresses in the thin region may be different from the bulk stress state. Further, an oxide layer on the surfaces may hinder the motion of dislocations. Nevertheless, in many cases the *in situ* TEM technique is a promising tool for investigations of dislocation–grain boundary interactions.

EXPERIMENTS

In situ deformation

Ni$_3$Al was prepared by arc-melting 99.99% pure Ni and 99.999% pure Al. The material was homogenized at 1100°C (1373 K) for 2 days, resulting in grain sizes of 1 mm. Miniature tensile specimens of 7 mm, with a thickness of 350 μm were cut out of the bulk material by spark erosion. There were two holes in the sample through which it was held by the pins of the two grips of the deformation holder. The sample was necked in the middle, so as to maximize the likelihood that the deformation would start near the future electron transparent region. Care was taken to have a grain boundary, preferably a coherent twin boundary, present in the middle of the sample.

Next, the sample had to be thinned to obtain an electron transparent region. First, the sample was ground to a thickness of 150 μm using a Gatan disc grinder and then the sample was dimpled on both sides of the location of the grain boundary, reducing the thickness locally from 150 μm to around 50 μm. This was done to increase the probability of having the grain boundary in the thin area. The last step of the preparation process was the final thinning of the specimen in a Struers Tenupol electropolishing unit, using a mixture of 70% methanol and 30% nitric acid at 0°C, at an applied voltage of 8 V.

For observation of the specimen, a JEM 200-CX was used, which was operated at 200 kV. The specimen was mounted in a special single tilt *in situ* deformation holder, built on principles taken from Kubin and Veyssière [10] (Fig. 1). In the deformation holder, the sample is strained by means of a vacuum system, which is operated from outside the microscope. In this way the sample is deformed at constant load. The processes during deformation could be monitored by a TV-system and could be recorded on video. The deformation was stopped before total disruption of the specimen. After the *in situ* deformation, specimens that promised to be interesting were shaped into 3 mm diameter discs by very cautious grinding, taking care that the thin area was protected. In this way they fitted in a double tilt holder and the defects could be analyzed in detail.

Computer modelling experiments

In the modelling study, Finnis–Sinclair potentials representing Ni$_3$Al [11] were used for the description of interatomic forces. For the simulations, the following procedure was used. First, the grain boundary was relaxed, using a standard gradient method; details are described elsewhere [12]. Secondly, a computational block for the relaxation of the dislocation near the grain boundary was constructed. The computational block of the relaxed grain boundary was extended, according to the periodicity of the CSL, to form a block of more than $40\,b \times 40\,b$ (b is the magnitude of the Burgers vector) perpendicular to the dislocation line. Next, the displacement field of a $\frac{1}{2}$[110] dislocation was imposed with its elastic center initially positioned at such a distance from the grain boundary that there was no strong effect of the grain boundary on the relaxation of the dislocation core.

Fig. 1. The *in situ* deformation holder with a sample mounted: 1: fixed grip, 2: sample, 3: thermocouple (not used), 4: moveable grip.

Along the dislocation line, periodic boundary conditions were applied. The anisotropic elastic solution (as if there was only one grain present) was used for the boundary conditions perpendicular to the dislocation line. The displacement field of $\frac{1}{2}[\bar{1}10]$ superpartial was imposed with its elastic centre near the boundary plane, connected by a ribbon of anti phase boundary (APB) to another superpartial at elastic equilibrium distance, according to the APB energy. The initial position of the core was always chosen such that dissociation would occur on the glide plane [13, 14]. The dislocation–grain boundary relaxation was carried out in the usual way for dislocation relaxation [15].

After relaxation of the dislocation core, a homogeneous shear strain was imposed on the computational block, corresponding to a shear stress, as prescribed by anisotropic elasticity theory (as if only the grain initially containing the dislocation was present). The shear stress was applied in the direction of the Burgers vector, such that the dislocation would move towards the grain boundary plane. The simulations started with imposing a shear strain corresponding to a small stress. Larger stresses were built up by repeating this process.

RESULTS

In situ deformation

In many samples, cracks (some of which were already present before the deformation started) were observed that had initiated at the edge of the thin foil, propagating along $\{111\}$ planes. Dislocations were often seen to be emitted from the crack tip, in the plane of the crack and sometimes also on inclined planes. In addition, observations were made of dislocations arriving from the bulk, although these observations were not so numerous. The dislocations from the bulk never arrived all on the same slip plane, but seemed to appear in slip bands. Quite frequently, the propagation of the crack occurred in a jerky type of motion and then, it was impossible to observe any dislocation motion.

In many of the specimens there was a grain boundary, often a coherent twin boundary ($\Sigma = 3$, 109.47° around $[110]$ with boundary plane $(\bar{1}11)$), visible in the electron transparent region. A number of observations were made of individual dislocations that had been emitted from cracks. Sometimes, dislocations arriving from the bulk impinged on twin boundaries and were arrested at the boundary plane. Cracks were seen that had grown through a twin boundary and had changed their direction of propagation upon crossing of the boundary plane.

Interaction with a $\Sigma = 3$ coherent twin boundary

One sample showed a crack which had grown during the *in situ* deformation to the close vicinity of a coherent twin boundary, but which had not crossed the boundary.

On the other side of the boundary, starting exactly from the line of intersection of the crack plane and the boundary plane, slip traces could be observed leading into the other grain, to a large number of dislocations that all had the same slip plane (Fig. 2).

This sample was chosen for further analysis in the double tilt holder. The rotation of the boundary under study could be described within the error margins as a 109.5° rotation around $[\bar{1}10]_{\mathrm{II}}$, characteristic for a twin boundary. By tilting to an edge-on position, the boundary plane was determined to be $(\bar{1}11)_{\mathrm{II}}$, which is equal to $(\bar{1}\bar{1}1)_{\mathrm{II}}$. The index II indicates the coordinate system of the grain containing the dislocations. The grain containing the crack is meant if no index is used. In a similar way, the plane of the crack was determined to be close to $(\bar{1}\bar{1}1)$ and the slip plane of the dislocations was determined to be $(\bar{1}\bar{1}1)_{\mathrm{II}}$. By the $\mathbf{g}\cdot\mathbf{b} = 0$ invisibility criterion, the Burgers vector of the dislocations was determined to be parallel to $[\bar{1}10]_{\mathrm{II}}$; this is the $[\bar{1}10]$ direction that is common to both grains. The line direction was

Fig. 2. The dislocation configuration that was found attached to the slip lines. 1: crack, 2: boundary plane, 3: dislocation array.

determined to be $[230]_{fl} \pm 13°$, which is close to the $[110]_{fl}$ screw direction.

Interaction with low-angle grain boundaries

In one sample, in the thin electron transparent region many low-angle grain boundaries were present, but no high angle grain boundaries were visible. In this sample there were only a few holes of approximately 5 μm in diameter and there were no cracks in the sample at all, contrary to most samples that contained a hole of about 50 μm in diameter and a few small initial cracks. The external force that had to be applied to cause deformation in the thin region was twice as high as usual for samples of the same thickness. This might be explained by the absence of stress concentrations because of cracks or large holes. During the experiment, many dislocations were seen gliding, almost exclusively in one slip band, in parallel planes. It was observed that at several places elongated stacking faults, hundreds of nanometers long, had been created at the intersections of the slip

Fig. 3. Stacking fault near a low-angle grain boundary (arrows), showing characteristic fringe contrast.

band with low-angle grain boundaries, see Fig. 3. The faults always lay at the same side of the boundaries: the direction of motion of the gliding dislocations always pointed from the boundary to the faults. Thus, it can be assumed that the faults have been created by interaction of the gliding dislocations with the dislocations in the boundary. Also at several other locations along the slip band, away from the intersections with low angle grain boundaries, gliding dislocations had formed faults. The deformation experiment was stopped after a crack had developed, originating from one of the holes. The sample was shaped into a 3 mm disc for further investigation in a double tilt holder. One of the intersections of the slip band with a low-angle grain boundary where faults had formed was chosen for detailed analysis. Three faults can be seen that are close to three dislocations in the low-angle grain boundary, at distances varying from less than 50–200 nm, see Fig. 4.

The foil normal was $[10\,3\,11] \pm 3°$, which is 11° from [101] and the foil thickness at the point of interest was 110 ± 15 nm. If we assume that the

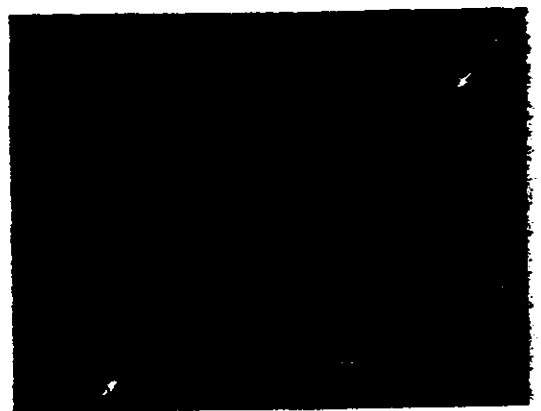

Fig. 4. Weak-beam micrograph of superlattice intrinsic stacking faults (SISFs) near a low-angle grain boundary. The arrows indicate the location of the low angle grain boundary or cell wall, consisting of an array of parallel dislocations spaced about 200 nm. Only one of the three SISFs can be seen fully; the other two are only partially in view.

Table 1. [illegible] for different reflections ($\mathbf{g}$'s) and fault vectors $\mathbf{R}_f$

$\mathbf{R}_f$	$\mathbf{g} = [00\bar{2}]$	$\mathbf{g} = [00\bar{2}]$
[illegible]	$-\frac{1}{3}$, [illegible]	$\frac{1}{3}$, [illegible]
[illegible]	$\frac{1}{3}$, [illegible]	$-\frac{1}{3}$, [illegible]

macroscopic tensile axis was perpendicular to the foil normal and parallel to the line connecting the two grips by which the sample was held, this axis could be determined to be $[4\bar{1}\bar{3}] \pm 10°$. It has to be noted that similar fault configurations close to a low-angle grain boundary have also been observed in thicker parts of the specimen, further down the same slip band. The average line direction of the dislocations constituting the low-angle grain boundary was $[025] \pm 5°$. The dislocations in the boundary had two different Burgers vectors: $[1\bar{1}0]$ or $[110]$. The dislocations that were close to the faults all had a Burgers vector $[1\bar{1}0]$. The dislocations in the boundary that had $\mathbf{b} = [110]$ were dissociated so widely into $\frac{1}{2}[110]$superpartial dislocations in the (100) plane, that the individual partials could be resolved in weak-beam (Fig. 4).

The plane of the faults was determined to be $(1\bar{1}1)$ by tilting the faults to an edge-on position. The fault vector $\mathbf{R}_f$ was determined to be $\pm\frac{1}{3}[1\bar{1}1]$ by applying the invisibility criterion $\alpha = 2\pi\mathbf{g}\cdot\mathbf{R}_f = n\cdot 2\pi$. However, for a fault of this type the positive and the negative fault vector are not equivalent. In one case, a $(1\bar{1}1)$ plane is removed (superlattice intrinsic stacking fault, SISF; this is a shear fault) and in the other case an extra $(1\bar{1}1)$ plane is added (superlattice extrinsic stacking fault, SESF; this is not a shear fault). The exact nature of the fault can be determined in the following way. The contrast of the edge fringe (the fringe at the intersection with the foil surface) in bright field images with $s = 0$ depends on the sign of $\sin\alpha$ [16]. If $\sin\alpha > 0$ the fringe is bright and if $\sin\alpha < 0$ the fringe is dark. The values of $\sin\alpha$ are listed in Table 1 for reflections which have been used to image the faults in bright field.

The experimental observations were that the edge fringe was dark for $\mathbf{g} = [002]$ and bright for $\mathbf{g} = [00\bar{2}]$, and therefore the fault vector $\mathbf{R}_f$ is $+\frac{1}{3}[1\bar{1}1]$. As the foil normal (pointing upwards) is close to $[101]$, $\mathbf{R}_f$ points to the upper surface of the foil. Thus the fault corresponds to a removal of one $(1\bar{1}1)$ plane and the fault is of intrinsic nature, a SISF.

From the direction of the slip traces left behind by the gliding dislocations it was deduced that the $(1\bar{1}1)$ plane of the faults is the same plane as the slip plane of the gliding dislocations. The faults are partially bounded by the intersection of their $(1\bar{1}1)$ plane and the upper surface of the foil and partially by dislocations with Burgers vector $\pm\frac{1}{3}[\bar{1}12]$ (Fig. 5).

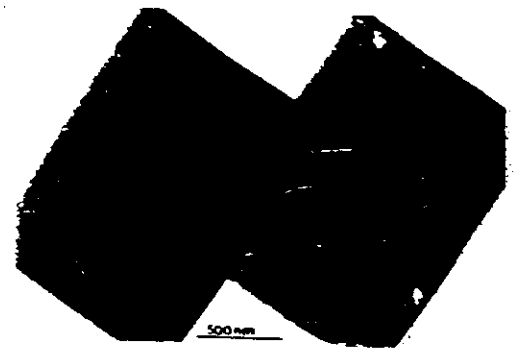

Fig. 5. Weak-beam micrograph of the dislocation partially bounding the faults of Fig. 4. Where not bounded by a dislocation, the faults are bounded by the surface of the thin foil. The fringe contrast of the faults is invisible for this imaging condition. The arrows indicate the location of the low angle grain boundary (cell wall).

The Burgers vector of the dislocations bounding the SISFs has been determined using the $\mathbf{g}\cdot\mathbf{b}$ invisibility criterion. The invisibility criterion for partial dislocations, such as a dislocation bounding a fault, is slightly different from that for perfect dislocations. For a Burgers vector of the type $\frac{1}{3}\langle 112\rangle$, the criterions for invisibility is $\mathbf{g}\cdot\mathbf{b} = 0$; $\pm\frac{1}{3}$ [16] and furthermore (for $s > 0$) $\mathbf{g}\cdot\mathbf{b} = -\frac{2}{3}$ [17]. Care was taken to use only reflections for which the fault is invisible, to prevent any uncertainty regarding visibility of the dislocation. The dislocations were invisible for $\mathbf{g} = [220]$ and for $\mathbf{g} = [13\bar{1}]$; they were visible for $\mathbf{g} = [022]$, $\mathbf{g} = [1\bar{3}\bar{1}]$ and $\mathbf{g} = [\bar{1}\bar{1}3]$. The $\mathbf{g}\cdot\mathbf{b}$ product for dislocations that can bound an SISF on $(1\bar{1}1)$ is given in Table 2.

From Table 2, it can be concluded that the Burgers vectors of the partial dislocations bounding the SISFs are $\pm\frac{1}{3}[\bar{1}12]$.

Computer modelling

Only the interaction of a $\frac{1}{2}[110]$ dislocation of pure screw character with the $\Sigma = 3$ $(\bar{1}11)$ ($\Theta = 109.47°$ around $[110]$) coherent twin boundary was simulated. In this set-up, transmission of the dislocation throughthe grain boundary is relatively easy, as no residue is left behind in the grain boundary plane. In the following, all Miller indices are in the coordinate system of the upper grain, unless otherwise indicated. In the kinematical simulations, the shear stress was applied onto the $(1\bar{1}1)$ plane.

It has to be emphasized that the symbols indicating the atom positions are drawn as if there is no dislocation present. The results for the kinematical

Table 2. $\mathbf{g}\cdot\mathbf{b}$ product for partial dislocations bounding an SISF on $(1\bar{1}1)$

$\mathbf{b}$	$\mathbf{g} = [220]$	$\mathbf{g} = [13\bar{1}]$	$\mathbf{g} = [022]$	$\mathbf{g} = [1\bar{3}\bar{1}]$	$\mathbf{g} = [\bar{1}\bar{1}3]$
$\pm\frac{1}{3}[12\bar{1}]$	2	2	2	−2	0
$\pm\frac{1}{3}[2\bar{1}1]$	2	2	0	0	−2
$\pm\frac{1}{3}[\bar{1}12]$	0	0	2	−2	2
$\pm\frac{1}{3}[\bar{1}\bar{1}1]$	0	−1	0	1	1

simulations are depicted using the differential displacement method [13]. This method indicates the relative displacement of each atom with respect to its neighbours in a certain crystallographic direction (usually the direction of the Burgers vector). If the absolute value of the relative displacement exceeds half of the periodicity of the lattice in that direction here, $\frac{1}{2}[110]$ was used), an integer number times the period is added or subtracted. The position of the APB is indicated by a line. The relative displacements are indicated by arrows drawn between the atoms.

The $\Sigma = 3$ boundary acted as an obstacle to dislocation motion. The leading $\frac{1}{2}[110]$ superpartial

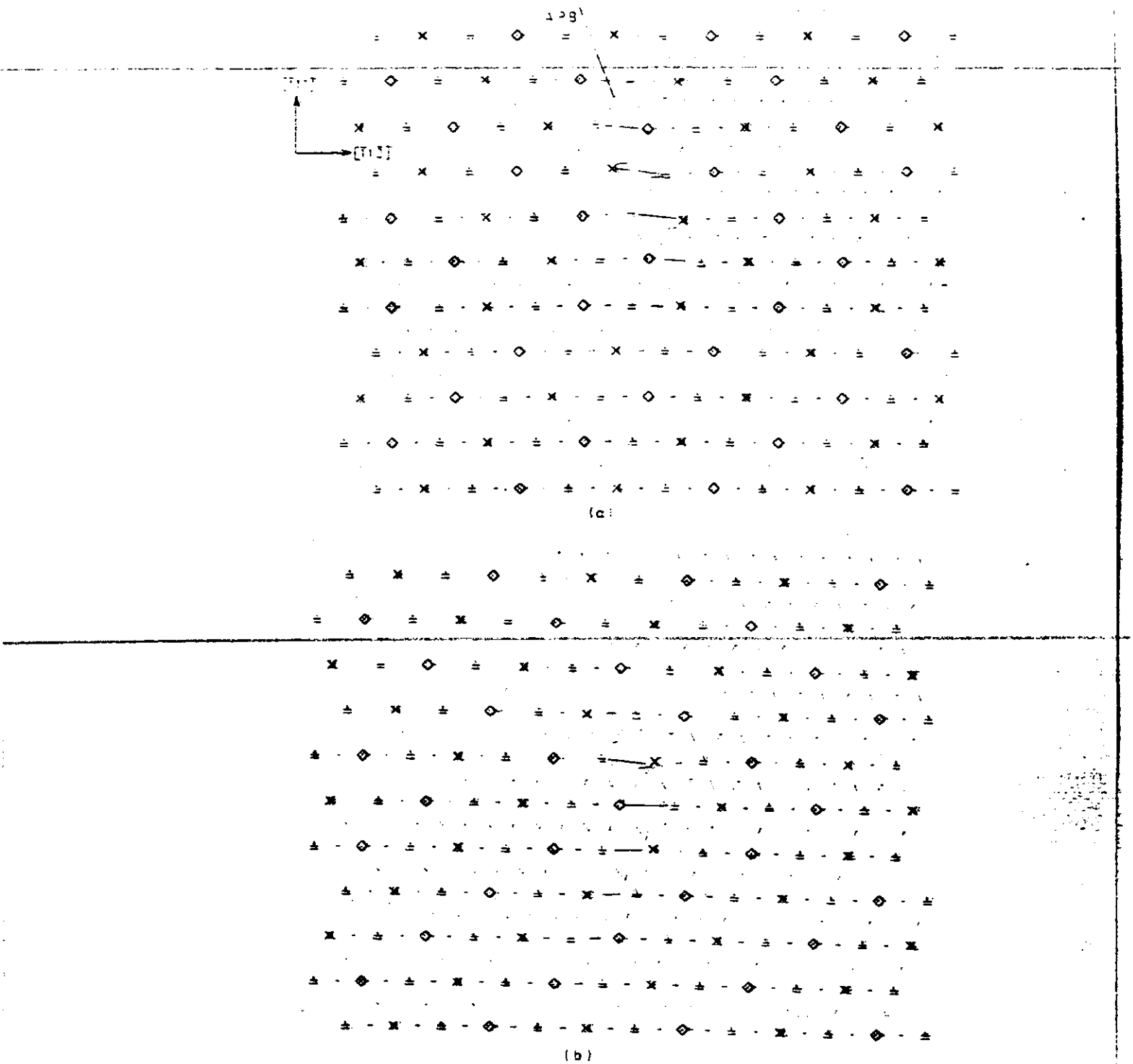

Fig. 6(a, b). *Caption on opposite page.*

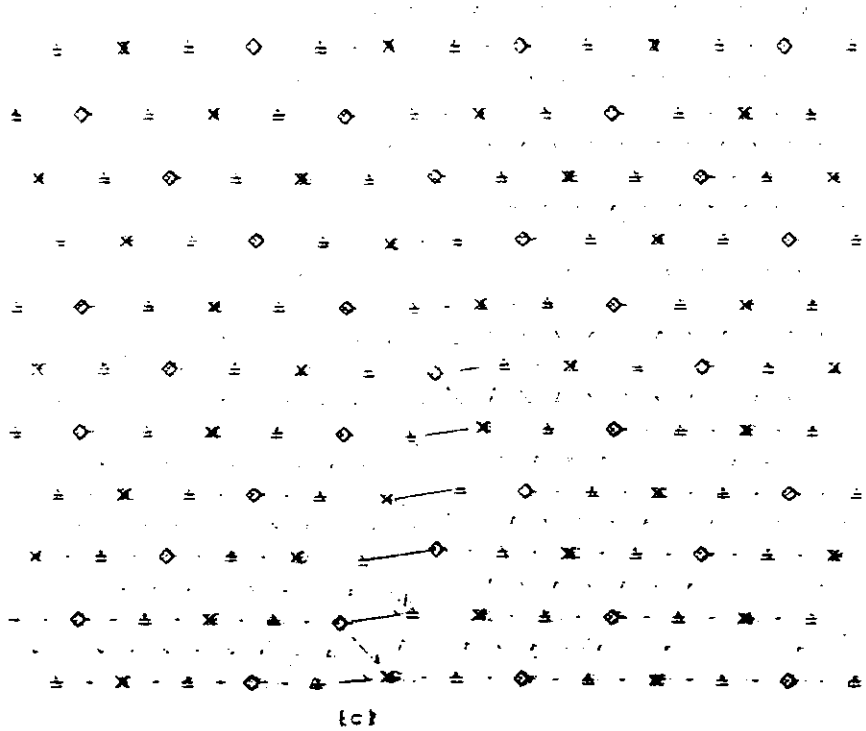

(c)

Fig. 6. (a–c) Three stages of the transmission through the $\Sigma = 3$ boundary in Ni_3Al. In these figures, a projection along [110] is shown. The different symbols indicate different heights. Following order: ◇, +, ×, △. The Al atoms are indicated by thicker lines. The position of the APB is indicated by a dashed line. The heights indicated by the symbols are heights before the dislocation was imposed.

dislocation was dissociated into two Shockley partials with very small separation. Upon arrival at the boundary plane, the leading Shockley partial was delayed and a slight decrease of the separation of the Shockleys could be observed. The trailing $\frac{1}{6}\langle 110]$ superpartial dislocation also approached the leading one. When the shear stress reached a level of 4 times the friction stress (the stress needed to start motion of the dislocation in perfect lattice), transmission occurred across the boundary into the symmetric slip-plane $(\bar{1}\bar{1}\bar{1})_B$ in the other grain, see Fig. 6.

DISCUSSION

Interaction with a $\Sigma = 3$ coherent twin boundary

The results of the TEM work show that cracks may emit dislocations parallel to their own plane during propagation. In the case of the sample containing a twin boundary that was analyzed in detail, the plane of the crack crossed a coherent twin boundary ahead of the crack and it might be evisaged that a number of dislocations was emitted from the crack tip in the $(\bar{1}\bar{1}\bar{1})$ plane and impinged on the boundary. The slip traces emanating on the other side of the boundary indicate that a number of dislocations has emerged from the boundary in the $(\bar{1}\bar{1}\bar{1})_B$ plane exactly at the point where the plane of the crack intersects with the boundary plane. Thus, it is probable that these dislocations have been emitted from the crack tip and have been transmitted through the grain boundary. As the $[\bar{1}10]$ direction is common to both grains, the Burgers vector could remain the same in both grains and no residue is left in the boundary. The line vector is parallel to the intersection of crack plane and outgoing slip plane and thus, transmission could occur without rotation of the dislocation line in the boundary plane. The large number of dislocations may indicate that there was a large force on the leading dislocation of a pile-up in front of the boundary, necessary to cause transmission of the dislocations to the other grain. Grain boundary sources of course cannot be ruled out completely as origin of the observed dislocations. However, very often, if operation of grain boundary sources is observed, there is generation of dislocations on many different slip planes [19] (our own observations in two other samples indicate the same); while here, all the dislocations are on one slip plane.

Interaction with low-angle grain boundaries

As low-angle grain boundaries consist of a dislocation network, the interaction between gliding lattice dislocations and low-angle grain boundaries is essentially a dislocation–dislocation interaction. In order to find an explanation for the formation of the SISFs, it is useful to know the type of the dislocations that were gliding in the slip band. Therefore, a number of dislocations that showed such a configuration that it could be expected that they had been gliding in the slip band was analyzed. Most of

the dislocations that were found in the slip band were screw dislocations with Burgers vector [011]. We may assume that the gliding dislocations in the slip band had Burgers vector [011]. This assumption can be supported as follows. If we suppose that the $\frac{1}{3}[\bar{1}12]$ dislocations bounding the SISFs were created by the gliding dislocations, the Burgers vector of the gliding dislocations could either be [011] or $[\bar{1}01]$, as only these dislocations are glissile in the $(1\bar{1}1)$ plane and at the same time can have $\frac{1}{3}[\bar{1}12]$ as one of their dissociation products. If we consider the tensile axis in the thin region to be the same as the macroscopic tensile axis, the Schmid factor for the [011] dislocations in the $(1\bar{1}1)$ plane is 0.38, while the Schmid factor for the $[\bar{1}01]$ dislocations is 0.15. Therefore we conclude that the gliding dislocations had Burgers vector [011]. As the dislocations in the slip band that were analyzed had mostly screw character, we may assume that the gliding dislocations also had screw character. Also it can be expected that the gliding dislocations were dissociated into two $\frac{1}{2}[011]$ superpartials, which is the dissociation that is usually found in Ni_3Al. See Fig. 7 for a schematic overview of the configuration.

Now, we consider the formation mechanism of the SISFs in more detail, see Fig. 8. A gliding dislocation intersects a dislocation in the cell wall. Although the dissociation of the perfect dislocation in the cell wall into superpartial dislocations is not clearly visible, we may assume that it is dissociated in the cell wall into two $\frac{1}{2}[1\bar{1}0]$s. Because of the intersection, 2 jogs have been created in the line of the gliding dislocation, which act as pinning points. As the separation between the two $\frac{1}{2}[1\bar{1}0]$s in the cell wall is very small, the jogs are very close to each other. The [011] dislocation will bow out at both sides of the pinning point under the influence of the stress (Fig. 8(b)). The leading $\frac{1}{2}[011]$ superpartial dislocation can be allowed to move under the applied stress in the following way: if a $\frac{1}{6}[21\bar{1}]$ Shockley partial dislocation moves from the trailing to the leading superpartial, the APB separating the $\frac{1}{2}[011]$ partials is transformed into SISF, which has much lower energy. By the exchange, the trailing $\frac{1}{2}[011]$ superpartial transforms to a $\frac{1}{3}[\bar{1}12]$ dislocation partially bounding the SISF (Fig. 8(c)).

In this way, the force keeping the two $\frac{1}{2}[011]$ dislocations together because of the high APB energy is greatly reduced as the SISF energy is much lower than the APB energy and thus, the leading $\frac{1}{2}[011]$, together with the $\frac{1}{6}[21\bar{1}]$ can proceed and then a large region of SISF can be formed (Fig. 8(d)). It might be envisaged that the termination of the SISF region develops in a similar way as the loop pinching mechanism described by Pak *et al.* [20]. See the text below for a brief description. In our case, we are dealing with a partial loop that is bounded by the foil surface and no next loop of SISF is created, but instead a new [011] perfect dislocation might be formed, which proceeds in the $(1\bar{1}1)$ plane.

There have been a number of other observations of SISFs in ordered alloys like Ni_3Al. Baker and Schulson [21] observed in Ni_3Al pairs of $\frac{1}{3}\langle 112\rangle$ dislocations with SISF between, separated around 100 nm. The $\frac{1}{3}\langle 112\rangle$ pairs had parallel Burgers vector and antiparallel line vector. These pairs were thought

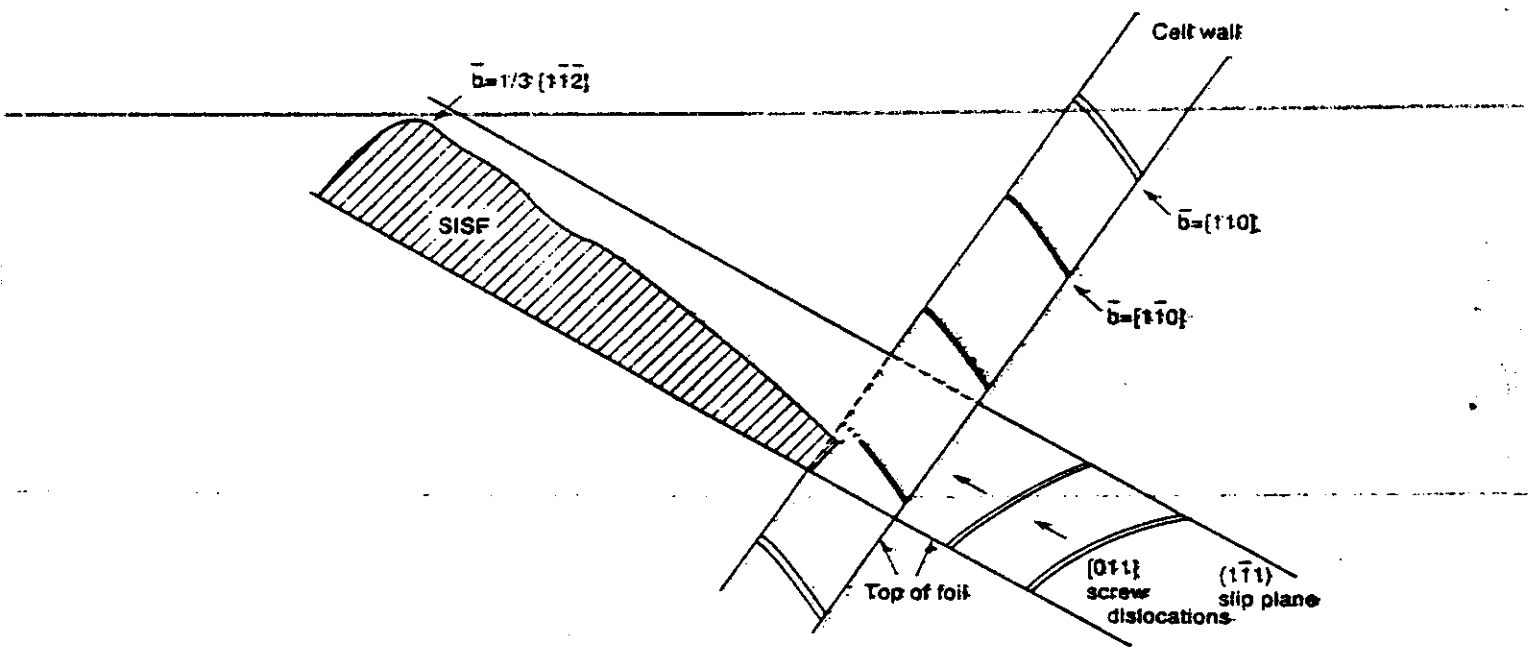

Fig. 7. Schematic view of the gliding dislocations, the low angle grain boundary (cell wall) and the SISF that is formed. The intersections of the slip plane of the gliding dislocations with the upper and lower surface of the thin foil are indicated. Also the intersection of the grain boundary plane and the foil surfaces has been indicated.

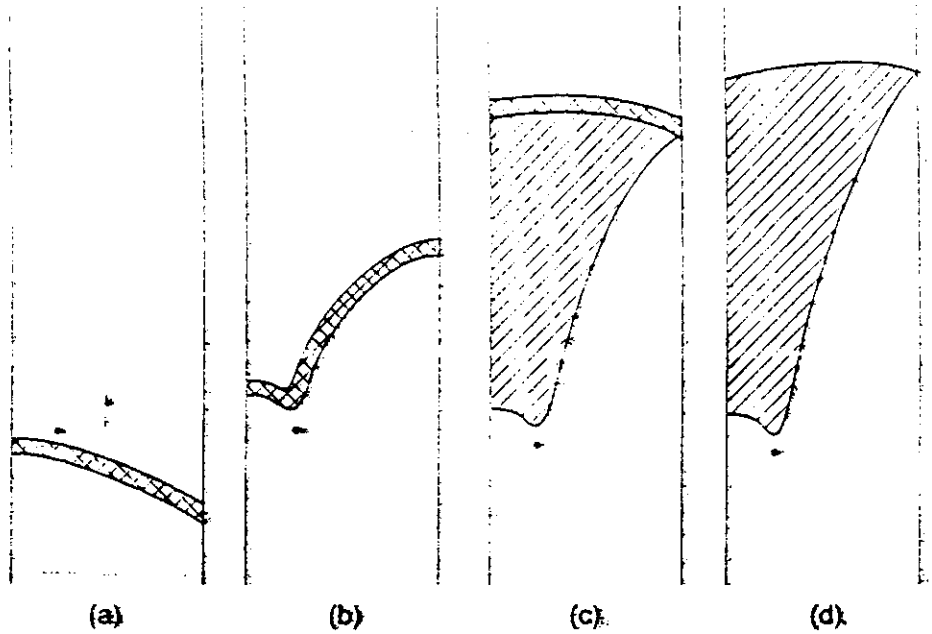

Fig. 8. Proposed SISF formation mechanism. Only the plane of the gliding dislocations is considered. The dislocation of the cell wall intersects the glide plane in a point, which is indicated. It is envisaged that the dislocation in the cell wall is actually dissociated into two superpartial dislocations very close to each other. Therefore the point actually represents two points very close to each other. (a) Dislocations gliding towards the intersection with the cell wall. The dislocations are each dissociated into two $\frac{1}{2}[0\bar{1}1]$ superpartial dislocations connected by a ribbon of anti phase boundary (APB; double hatched). (b) After intersection, the gliding dislocation has a two jogs in its line and because of the pinning by the jogs it bows out under influence of the applied stress. (c) By the exchange of a $\frac{1}{6}[2\bar{1}\bar{1}]$ Shockley partial dislocation between the trailing $\frac{1}{2}[0\bar{1}1]$ superpartial dislocation and the leading $\frac{1}{2}[0\bar{1}1]$ superpartial, the region of APB (double hatched) between the partials is transformed into SISF (single hatched). (d) Because of the lower energy of the SISF the leading partial is allowed to move further in the glide direction.

to be elongated dislocation loops that were truncated because of the thinning process during preparation of the foil. Some observations were made of rows of loops of SISF of several hundred nm long. Pak *et al.* [20] made observations in Ni_3Ga, which is a very similar material to Ni_3Al, of widely extended SISFs with lengths of several hundreds of nanometers to a few μm, elongated along $\langle 110\rangle$ directions and bounded by $\frac{1}{3}\langle 112\rangle$ type partial dislocations. Veyssière *et al.* [22] made observations of two $\frac{1}{2}\langle 110\rangle$ superpartials that were dissociated in a $\{100\}$ plane, connected by a ribbon of APB. Parts of one of the $\frac{1}{2}\langle 110\rangle$ dislocations had dissociated in an inclined $\{111\}$ plane into a $\frac{1}{6}\langle 112\rangle$ type edge Shockley partial and a $\frac{1}{3}\langle 112\rangle$ type partial dislocation. These two dislocations were connected by a ribbon of SISF on the $\{111\}$ plane.

Several explanations have been put forward for the SISF formation. Pak *et al.* [20] explained the formation of loops bounding SISF's by means of an expanding perfect dislocation loop, which partially dissociates into two $\frac{1}{3}\langle 112\rangle$ partial dislocations. Upon further expansion of the perfect loop, the SISF is elongated and finally, part of the SISF is pinched off and a faulted loop containing the SISF is created. Kear *et al.* [23, 24] discussed mechanisms by which gliding dislocations on intersecting slip planes could react and they showed that an SISF is formed in certain reactions. The mechanism described by Kear *et al.* is essentially a dislocation interaction mechanism involving two different slip planes, while the mechanism described by Pak *et al.* is essentially a single slip plane mechanism. Pak *et al.* do not go further into the reason of the initial dissociation of part of the perfect dislocation loop into $\frac{1}{3}\langle 112\rangle$ partial dislocations. The SISF formation in our observations resembles the Pak *et al.* mechanism, as only one slip plane is involved. The creation of jogs in the line of the gliding dislocations because of the intersection with the dislocations in the cell wall could be the reason for the dissociation into $\frac{1}{3}\langle 112\rangle$ partials under influence of the applied stress.

Comparison between modelling results and experimental observations

Our experimental observations of the interaction with the $\Sigma = 3$ coherent twin boundary can be compared to the computer modelling results, see also [4, 5]. The dislocation-grain boundary system that was studied is exactly the same as the system that is studied here experimentally and therefore a one-to-one comparison is possible. The interaction mechanism that is observed in Ni_3Al in the simulations is the same as that which is observed in the *in situ* defor-

mation experiment. The magnitude of the stress at which transmission occurs cannot be compared so easily, as there is no experimental observation of a pile-up of dislocations against the grain boundary. From the number of dislocations in a pile-up and their spacing, the effective stress on the first dislocation near the boundary plane could be calculated. The friction stresses that are observed in the simulations are high in comparison with experiment and therefore the stresses that are necessary for transmission can be expected to be high as well.

The question may arise whether the observed behaviour is specific to Ni_3Al or exhibits a general feature of f.c.c. materials or of other $L1_2$ structured materials like Cu_3Au.

Observations of the same dislocation–grain boundary system were made in type 304 steel [25] and in 310 stainless steel [26]. Both materials have the f.c.c. structure. In 304 type stainless steel, a configuration in slightly deformed materials was observed which showed a pile-up of dislocations one side of the boundary and dislocations which appeared to have emerged on the other side. It was concluded that transmission through the twin boundary had taken place, equal to the results reported in this paper. The same mechanism of transmission of the same type of dislocations through the same boundary was observed in 310 steel during *in situ* deformation experiments [26].

However, in Cu_3Au absorption in the boundary plane was observed [5, 27], although there were a number of observations of transmissions as well. A possible explanation for the tendency to absorption could be found in a lower value of the energy of the ordering fault in the grain boundary plane between two $\frac{1}{2}\langle 110\rangle$ superpartial dislocations compared with the value of the APB between the superpartials in the bulk: i.e. in the order of 20 mJ/m^2 [4]. Thus regarding this energy difference absorption in the boundary might be expected, which of course is in contrast to f.c.c. materials since an ordering fault is not present, neither in the bulk nor grain boundary.

The main feature of Ni_3Al as compared with f.c.c. and other $L1_2$ materials like Cu_3Au lies in the stress level at which transmission through the boundary occurs [4]. The two superpartial dislocations in $L1_2$ constituting the arriving dislocation will decrease their separation in response to the applied stress, when the leading superpartial dislocation is halted at the boundary. In this way stress concentrations near the boundary will be generated which will increase upon increasing ordering tendency. Since the ordering tendency in Ni_3Al is much larger than in Cu_3Au the boundary in Ni_3Al will act as a much stronger obstacle for dislocation transmission.

CONCLUSIONS

Samples of Ni_3Al have been strained *in situ* in a TEM. The results of the *in situ* straining indicate that $\langle 110\rangle$ screw dislocations impinging on a $\Sigma = 3$ coherent twin boundary that have a Burgers vector that is parallel to the grain boundary plane can be transmitted to the symmetric slip plane in the other grain under influence of an applied stress. A one-to-one comparison with the results of a computer modelling study of exactly the same system in Ni_3Al can be made and the experiment agrees with the simulations. Also, observations were made of superlattice intrinsic stacking faults (SISF) that were formed as a result of the interaction between gliding dislocations and the dislocations of a low angle grain boundary (cell wall). The creation of jogs in the line of the gliding dislocation may be the cause of the SISF formation.

Acknowledgements—This research is part of the research program of the Foundation for Fundamental Research on Matter (F.O.M.—Utrecht, The Netherlands) and has been made possible by financial support from The Netherlands Organization for Research (N.W.O.—The Hague, The Netherlands).

REFERENCES

1. K. Aoki and O. Izumi, *Nippon kink. Gakk.* 43, 1190 (1979).
2. I. Baker, E. M. Schulson and J. A. Horton, *Acta metall.* 35, 1533 (1987).
3. S. Hanada, T. Ogura, S. Watanabe, O. Izumi and T. Masumoto, *Acta metall.* 34, 13 (1986).
4. B. J. Pestman, J. Th. M. De Hosson, V. Vitek and F. W. Schapink, *Phil. Mag. A* 64, 951 (1991).
5. B. J. Pestman, J. Th. M. De Hosson, V. Vitek, F. D. Tichelaar and F. D. Schapink, *Alloy Phase Stability and Design* (edited by G. M. Stocks, D. P. Pope and A. F. Giamei), pp. 186, 253. MRS (1991).
6. J. J. Hauser and B. Chalmers, *Acta metall.* 9, 802 (1961).
7. W. D. Brentnall and W. Rostoker, *Acta metall.* 13, 187 (1965).
8. D. J. Dingley and R. C. Pond, *Acta metall.* 27, 667 (1979).
9. M. Elkajbaji and J. Thibault-Desseaux, *Phil. Mag. A* 58, 325 (1988).
10. L. P. Kubin and P. Veyssière, *Proc. 10th Int. Cong. Electron Microscopy*, Hamburg, W. Germany, p. 531. Deutsche Gesellschaft für Elektronenmikroskopie e.V. (Battelle-Institut e.V.): Frankfurt/Main (1982).
11. V. Vitek, G. J. Ackland and J. Cserti, *Alloy Phase Stability and Design* (edited by G. M. Stocks, D. P. Pope and A. F. Giamei), pp. 186, 237. MRS (1991).
12. A. P. Sutton and V. Vitek, *Phil. Trans. R. Soc. A* 309, 37 (1983).
13. D. Farkas and E. J. Savino, *Scripta metall.* 22, 557 (1988).
14. M. Yamaguchi, V. Paidar, D. P. Pope and V. Vitek, *Phil. Mag. A* 45, 867 (1982).
15. Z. S. Basinski, M. S. Duesbery and R. Taylor, *Phil. Mag.* 22, 1201 (1970).
16. P. B. Hirsch, A. Howie, R. B. Nicholson, D. W. Pashley and M. J. Whelan, *Electron Microscopy of Thin Crystals*, p. 156. Butterworths, London (1965).
17. J. M. Silcock and W. J. Tunstall, *Phil. Mag.* 10, 361 (1964).
18. V. Vitek, R. C. Perrin and D. K. Bowen, *Phil. Mag.* 21, 1049 (1970).

19. G. M. Bond, I. M. Robertson and H. K. Birnbaum, *J. Mater. Res.* **2**, 436 (1987).
20. H. R. Pak, T. Saburi and S. Nenno, *Scripta metall.* **10**, 1063 (1976).
21. I. Baker and E. M. Schulson, *Physica status solidi (a)* **85**, 481 (1984).
22. P. Veyssière, J. Douin and P. Beauchamp, *Phil. Mag. A* **51**, 289 (1985).
23. B. H. Kear, A. F. Giamei and J. M. Oblak, *Scripta metall.* **4**, 567 (1970).
24. B. H. Kear, J. M. Oblak and A. F. Giamei, *Metall. Trans.* **1**, 2477 (1970).
25. W. A. T. Clark, R. H. Wagoner, *Dislocations in Solids* (edited by H. Suzuki, T. Ninomiya, K. Sumino and S. Takeuchi), p. 647. Univ. of Tokyo Press (1985).
26. T. C. Lee, I. M. Robertson and H. L. Birnbaum, *Metall. Trans.* **21A**, 2437 (1990).
27. F. D. Tichelaar and F. W. Schapink, *Phil. Mag. A* **62**, 53 (1990).